Classification of visual cortex plasticity phenotypes following treatment for amblyopia

Justin L. Balsor[1] David G. Jones[2] Kathryn M. Murphy[1,3]

[1] McMaster Integrative Neuroscience Discovery and Study (MiNDS) Program, McMaster University, Hamilton, ON, L8S 4K1, Canada
[2] Pairwise Affinity Inc, Dundas, ON, L9H 2R9, Canada
[3] Department of Psychology, Neuroscience & Behavior, McMaster University, Hamilton, ON, L8S 4K1, Canada

Correspondence should be addressed to Kathryn M. Murphy; kmurphy@mcmaster.ca

Kathryn Murphy, Department of Psychology, Neuroscience & Behavior, McMaster University, McMaster University, 1280 Main Street West, Hamilton, ON L8S 4K1, Canada.

Authors' contributions: JB Designed research, performed research, analyzed data, wrote/revised the paper; DJ analyzed data, revised the paper; KM designed research, performed research, analyzed data, wrote/revised the paper.

Acknowledgements: We thank Kyle Hornby and Dr Brett Beston for assistance with data collection.

Funding Sources: NSERC Grant RGPIN-2015-06215 awarded to KM, Woodburn Heron OGS awarded to JB.

Data Availability: The data used to support the findings of this study are available from the corresponding author upon request.

Abstract

Monocular deprivation (MD) during the critical period (CP) has enduring effects on visual acuity and the functioning of the visual cortex (V1). This experience-dependent plasticity has become a model for studying the mechanisms, especially glutamatergic and GABAergic receptors, that regulate amblyopia. Less is known, however, about treatment-induced changes to those receptors and if those changes differentiate among treatments that support good recovery of acuity versus persistent acuity deficits. Here we studied the effects of 3 treatments for MD started during the CP (n=24, 10 male and 14 female). Two treatments (reverse occlusion -- RO, binocular deprivation -- BD) resulted in poor acuity, but one treatment (binocular vision --BV) promoted good acuity. We classified plasticity phenotypes using the expression of a collection of glutamatergic and GABAergic receptor subunits in V1. Analyzing individual proteins showed an intricate pattern of changes, but principal component analysis identified features that we used to construct the plasticity phenotypes and classify treatments into clusters suggesting adaptive versus maladaptive plasticity. The RO plasticity phenotype was similar to an adult pattern with high expression of GluA2, while the BD phenotypes were dominated by $GABA_A\alpha1$, highlighting that multiple plasticity phenotypes can underlie persistent acuity deficits. In contrast, BV for 2-4 days promoted recovery of a phenotype resembling CP plasticity, but only one feature, the GluN2A:GluA2 balance, returned to normal levels. This suggests that balancing homeostatic and Hebbian mechanisms is needed for good visual recovery. These findings and the plasticity phenotyping approach may be useful for classifying different forms of persistent amblyopia and identifying new treatment targets.

Keywords: amblyopia, neuroplasticity, GABA, NMDA, AMPA, phenotype, high-dimensional, treatment, recovery, binocular vision, reverse occlusion, binocular deprivation

Introduction

Since the earliest demonstrations that monocular deprivation (MD) during a critical period (CP) cause ocular dominance plasticity and acuity loss[1]-[3] this model has been used to deepen our understanding of the neural changes associated with amblyopia. There have been fewer studies, however, about cortical changes associated with the acuity deficits that often persist after treatment for amblyopia[4]-[8]. Here we classified the expression patterns (phenotypes) of a collection of synaptic proteins that regulate experience-dependent plasticity and asked if treatments that promote good versus poor acuity reinstate CP-like plasticity phenotypes in visual cortex (V1).

Many animal studies have highlighted the role of glutamatergic and GABAergic mechanisms for regulating plasticity during the CP[9]-[15]. For example, the subunit composition of AMPA, NMDA, and $GABA_A$ receptors regulate the bidirectional nature of ocular dominance plasticity[16]-[21]. Some of the changes caused by MD include delaying the maturational shift to more GluN2A-containing NMDARs[22], [23], and accelerating the expression of $GABA_A\alpha1$-containing $GABA_A$Rs[20], [23]. Together those changes likely decrease signal efficacy and dysregulate the spike-timing dependent plasticity that drives long-term depression (LTD) and weakens deprived eye response[24]. Furthermore, silencing activity engages homeostatic mechanisms that scale the responsiveness of V1 neurons by inserting GluA2-containing AMPAR into the synapse[25]. Importantly, many of the receptor changes have been linked with specific acuity deficits[26], [27] suggesting that visual outcomes may reflect changes to a collection of glutamatergic and GABAergic receptor subunits that together represent a plasticity phenotype for V1.

Animal studies of amblyopia have also identified treatments that promote good versus poor recovery of acuity after MD, and these can be used to compare adaptive versus maladaptive plasticity mechanisms. For example, a model of full-time patching therapy (reverse occlusion, RO) gives a competitive advantage to the deprived eye that promotes an ocular dominance shift. The acuity recovered by the deprived-eye, however, is transient, and can be lost within hours of introducing binocular vision[6]-[8]. Similarly, closing both eyes after MD to test a form of binocular deprivation therapy (BD) leads to poor acuity in both eyes even after months of binocular vision[28]. In contrast, using only binocular vision (BV) after MD to engage cooperative plasticity promotes both physiological recovery[29] and long-lasting visual recovery in both eyes[27].

Here we quantified expression of glutamatergic and GABAergic receptor subunits in V1 of animals reared with MD and then treated to promote either good visual recovery (BV) or persistent bilateral amblyopia (RO, BD). We compared subunit expression among the treatment groups and with normally developing or MDed animals. Next, we applied a data-driven approach to identify plasticity features in the pattern of subunit expression and to construct plasticity phenotypes. Finally, we used cluster analysis to classify plasticity phenotypes associated with good versus poor acuity and analyzed those to determine which features suggest the recovery of adaptive versus maladaptive plasticity mechanisms.

Materials & Methods

Animals & Rearing Conditions

All experimental procedures were approved by the McMaster University Animal Research Ethics Board. We quantified the expression of 7 glutamatergic and GABAergic synaptic proteins in V1 of cats reared with MD from eye opening until 5 weeks of age and then given one of 3 treatments: RO for 18d, BD for 4d, or BV for either 1hr, 6hrs, 1d, 2d or 4d (n=7, 4 male and 3 female) (Figure 1). The length of RO and BD were selected to match previous studies that found poor acuity in both eyes[7], [8], [30]. The raw data collected previously[23] was also used. Those data were from animals reared with normal binocular vision until 2, 3, 4, 5, 6, 8, 12, 16, or 32 wks of age (n=9 animals, 2 male and 7 female), or MD from eye opening (6-11d) to 4, 5, 6, 9, or 32 wks (n=8 animals, 4 male and 4 female) (Figure 1).

MD was started at the time of eye-opening by suturing together the eyelid margins of one eye (5-0 Coated VICRYL Ethicon P-3) using surgical procedures described previously[8]. Sutures were inspected daily to ensure the eyelids remained closed. At 5 weeks of age, the period of MD was stopped and either BV was started by carefully parting the fused eyelid margins, RO was started by opening the closed eye and closing the open eye or BD was started by closing the open eye. All of these surgical procedures were done using gaseous anesthesia (isoflurane, 1.5-5%, in oxygen) and aseptic surgical techniques.

At the end of the rearing condition animals were euthanized using sodium pentobarbital injection (165mg/kg, IV), and transcardially perfused with cold 0.1M phosphate buffered saline (PBS) (4˚C; 80-100 ml/min) until the circulating fluid ran clear. The brain was removed from the

skull and placed in cold PBS. A number of tissue samples (2 mm x 2 mm) were taken from the regions of V1 representing the central, peripheral and monocular visual fields (Figure 1c). Each tissue sample was placed in a cold microcentrifuge tube, flash frozen on dry ice, and stored in a -80˚C freezer.

Synaptoneurosome preparation

Synaptoneurosomes were prepared according to a subcellular fractionation protocol[16], [31]. The tissue samples were suspended in 1 ml of cold homogenization buffer (10 mM HEPES, 1 mM EDTA, 2 mM EGTA, 0.5 mM DTT, 10 mg/l leupeptin, 50 mg/l soybean trypsin inhibitor, 100 nM microcystin and 0.1mM PMSF), and homogenized in a glass-glass Dounce tissue homogenizer (Kontes, Vineland, NJ, USA). Homogenized tissue was passed through a 5µm-pore hydrophobic mesh filter (Millipore, Billerica, MA), centrifuged at low-speed (1,000xg) for 20 min, the supernatant was discarded, and the pellet was re-suspended in 1ml cold homogenization buffer. The sample was centrifuged for 10 min (1000x*g*), the supernatant was discarded, and the pellet was re-suspended in 100µl boiling 1% sodium-dodecyl-sulfate (SDS). Samples were heated for 10 min and then stored at -80˚C.

Total protein concentrations were determined for each sample and a set of protein standards using the bicinchoninic acid (BCA) assay (Pierce, Rockford, IL, USA). A linear function was fit to the observed absorbance values of the protein standards relative to their expected protein concentrations. If the fit was less than R^2=0.99, the assay was re-done. The slope and the offset of the linear function were used to determine the protein concentration of each sample and then the samples were diluted to 1 µg/µl with sample (M260 Next Gel Sample loading buffer 4x, Amresco) and Laemmli buffer (Cayman Chemical). A control sample was made by combining a

small amount from each sample to create an average sample that was run on every gel. Each sample was run twice in the experiment.

Immunoblotting

Synaptoneurosome samples and a protein ladder were separated on 4-20% SDS-PAGE gels (Pierce, Rockford, IL) and transferred to polyvinyldenine fluoride (PVDF) membranes (Millipore, Billerica, MA). The blots were blocked in PBS containing 0.05% Triton-x (Sigma, St. Louis, MO) (PBS-T) and 5% skim milk (wt/vol) for 1 hour. Blots were then incubated overnight at 4˚C with constant agitation in one of the 7 primary antibodies (Table 1), and washed with PBS-T (Sigma, St. Louis, MO) (3 x 10 min).

Table1: List of primary antibody concentrations

Antibody	Concentration	Company	Lot Number	Location	RRID
anti-GluN1	1:2000	BD Biosciences Pharmingen	556308	San Diego, CA	RRID:AB_396353
anti-GluN2A	1:2000	Millipore Sigma	24826	Burlington, MA	RRID: AB_95169
anti-GluN2B	1:2000	Millipore Sigma	28629	Burlington, MA	RRID: AB_2112925
anti-GluA2	1:1000	Thermo Fisher		Waltham, MA	RRID: AB_2533058
anti-$GABA_A\alpha1$	1:500	Santa Cruz Biotechnology	L3102	Santa Cruz, CA	
anti-$GABA_A\alpha3$	1:2000	Millipore Sigma		Burlington, MA	
anti-Synapsin	1:2000	Thermo Fisher		Waltham, MA	

The appropriate secondary antibody conjugated to horseradish peroxidase (HRP) (1:2000; Cedarlane laboratories LTD, Hornby, ON) was applied to membranes for 1 hour at room temperature, then blots were washed in PBS (3 x 10 min). Bands were visualized using enhanced chemiluminescence (Amersham, Pharmacia Biotech, Piscataway, NJ) and exposed to autoradiographic film (X-Omat, Kodak, Rochester, NY). After each exposure blots were stripped (Blot Restore Membrane Rejuvenation kit (Chemicon International, Temecula, CA, USA)) and probed with the next antibody so each blot was probed for all 7 antibodies (Figure 1d).

Analysis of Protein Expression

The autoradiographic film and an optical density wedge (Oriel Corporation, Baltimore, MD) were scanned (16 bit, AFGA Arcus II, Agfa, Germany), and the bands were identified based on molecular weight. The bands were quantified using densitometry and the integrated grey-level of the band was converted into optical density units (OD) using custom software (MATLAB, The Mathworks, Inc., Natick, Massachusetts). The background density between the lanes was subtracted from each band and the density of each sample was normalized relative to the control sample run on each gel (sample band density/control band density).

The data were normalized relative to the average expression of the 5wk normal cases and plotted either as histograms to compare expression levels among the 5wk Normal, 5wk MD, RO, and BD animals or as scatterplots to follow expression changes over the 5 different lengths of BV. Table 2 summarizes the number of tissue samples and replication of runs for the 5wk Normal, 5wk MD and recovery conditions across the 3 regions of V1, and 7 proteins that were studied. The data analysis study design is summarized in Figure 2.

Table 2: The number of tissue samples and runs for each treatment condition, V1 region and protein studied. Rows summarize the number of runs from the Central (C), Peripheral (P), and Monocular (M) regions of V1 within a rearing condition. The columns list each of the 7 proteins analyzed using Western blotting. Column sums detail the number of runs across rearing conditions and cortical areas. The number of replications is listed for Normal animals in Table 2-1, and MD animals in Table 2-2.

Condition	Region	GluN1	GluN2A	GluN2B	$GABA_A\alpha1$	$GABA_A\alpha3$	GluA2	Synapsin
5wk Normal	C	4	4	4	4	4	4	4
	P	16	16	16	15	16	16	16
	M	4	4	4	4	4	4	4
5wk MD	C	6	6	6	6	6	6	4
	P	18	18	18	18	18	18	12
	M	5	5	5	5	5	5	4
18d RO	C	4	4	4	4	4	4	4
	P	19	19	19	19	19	14	14
	M	3	3	3	3	3	2	2
4d BD	C	6	6	5	6	5	6	5
	P	18	18	17	16	18	18	17
	M	4	4	3	4	4	4	3
1hr BV	C	4	4	4	4	4	4	4
	P	16	16	16	16	16	16	16
	M	4	4	4	4	4	4	3
6hr BV	C	4	4	4	4	4	4	4
	P	16	16	16	16	16	16	16
	M	4	4	4	4	4	4	4
1d BV	C	4	2	4	4	4	4	4
	P	16	13	16	16	16	16	16
	M	4	4	4	4	4	4	4
2d BV	C	4	4	4	3	4	4	2

	P	15	15	15	15	14	15	12
	M	4	4	4	4	4	4	4
4d BV	C	4	4	4	4	4	4	4
	P	12	12	12	12	12	12	12
	M	4	4	4	4	4	4	4
SUM		222	217	219	218	220	216	198

We analyzed heterogeneity in protein expression within a group by calculating an index of dispersion, the variance-to-mean ratio (VMR), for each protein and rearing condition. Proteins with VMR <1 were classified as under-dispersed, VMR=1 randomly dispersed, and VMR >1 were over-dispersed. We used this measure to compare among groups and assess if a rearing condition changed the variability of protein expression to make the group more or less heterogeneous.

Protein Indices

To examine the balance between developmentally and functionally related pairs of glutamatergic and GABAergic receptor subunits, we calculated a set of 3 indices (difference ratios). The indices included: GluA2:GluN1, GluN2B:GluN2A, $GABA_A\alpha3$:$GABA_A\alpha1$, which ranged from -1 to 1. The mean and SEM for each index was plotted as either a histogram (5wk Normal, 5wk MD, BD, RO) or scattergram (BV).

Protein Network Analysis

A network analysis of protein expression was done for each rearing condition by calculating the pairwise Pearson's R correlations among the 7 proteins using the *rcorr* function in the Hmisc package in R[32]. The networks were visualized as correlation matrices (*heatmap2* function in

gplots[33]) and the proteins were ordered (dendextend package[34]) using the seriation package[35] to place proteins with similar patterns of correlations nearby in the dendrogram. Significant correlations were identified using Bonferroni corrected p-values and indicated by asterisks on the cell in the correlation matrix.

Modeling Population Receptor Decay Kinetics for NMDARs and $GABA_A$Rs

The subunit composition of NMDARs and $GABA_A$Rs determines the decay kinetics of the receptor[36], [37] and so we used that information to build a model for the decay kinetics of a population of receptors for each of the rearing conditions. The decay kinetics of the most common NMDAR composition, triheteromeric receptors containing GluN2A and 2B is 50ms±3ms, while diheteromers NMDARs containing only GluN2B are slower (2B=333ms±17ms) and those containing only GluN2A are faster (2A=36ms±1ms) [36]. The decay kinetics of $GABA_A$Rs with both α1 and α3 subunits is 49ms±23ms while receptors with only the α3 subunit are slower (129.0ms±54.0ms) and only α1 are faster (42.2ms±20.5ms) [37].

We used the relative amounts of GluN2A and 2B, or $GABA_A$α1 and α3, as inputs to the model. Receptors containing GluN2A and 2B or $GABA_A$α1 and α3 are the most common in the cortex, so the model maximized the number of these pairs which was limited by the subunit with less expression. The remaining proportion of the highly expressed subunit was divided by 2 and used to model the number of pairs for those receptors (2A:2A or 2B:2B; α1:α1 or α3:α3) in the population. The population decay kinetics were then modeled by inserting the relative amounts of the subunits into these formulas:

NMDAR kinetics (([2A:2B]×50ms)+([2A]×36ms)+([2B]×333ms)) / ([2A:2B]+[2A]+[2B]);

$GABA_AR$ kinetics (([α1:α3]×49ms)+([α1]×42.2ms)+([α3]×129ms)) / ([α1:α3]+[α1]+[α3]).

For example, a sample where GluN2A was 35% and 2B was 65% of the total NMDAR subunit population and would have population kinetics of 135ms.

(([(0.65-0.35)/2]×50ms)+([(0)/2]×36ms)+([0.35/2]×333ms)) / ([(0.65-0.35)]+[(0)/2]+[0.35])= 135ms.

First, we plotted scattergrams of the average NMDAR and $GABA_AR$ decay kinetics for normal animals and each treatment condition. The development of decay kinetics for normal animals was described using an exponential decay function, while changes in kinetics with increasing lengths of BV were fit by either exponential decay or sigmoidal curves. Next, we compared the relationship between NMDAR and $GABA_AR$ kinetics by plotting both on one graph.

Principal component analysis

We used principal component analysis (PCA) to reduce the dimensionality of the data, identify potential biological features, and create plasticity phenotypes. We applied PCA following procedures we used previously[23], [38], [39] and included data from all of the normal animals and MDs as well as the 3 recovery conditions. We assembled protein expression for GluA2, GluN1, GluN2A, GluN2B, $GABA_Aα1$, $GABA_Aα3$, and Synapsin into an *mxn* matrix. The *m* columns represented the 7 proteins and the *n* rows were the average protein expression for each of the 12-14 samples from an animal. For a few of the rows data was missing from a single cell and so those samples were omitted for a total of *n*=279 rows in the matrix and 1,953 observations.

The data were centered by subtracting the mean column vector and applying a singular value decomposition (SVD) to calculate the principal components (R Studio). SVD represents the expression of all 7 proteins within a single tissue sample as a vector in high dimensional space and the PCA identifies variance captured by each dimension in that "protein expression space". The first 3 dimensions accounted for 82% of the total variance and were used for the next analyses.

We plotted the basis vectors for the first 3 dimensions (Dim) and used the weight, quality (cos^2) and directionality of each protein, as well as known protein interactions to help identify potential biological features accounting for the variance. We identified 9 potential features (7 new and 2 indices already analyzed), calculated those features for each sample and correlated each feature with Dim1, Dim2 and Dim3 to create a correlation matrix (see results). The p-values for the correlations were Bonferroni corrected and significant correlations were used to identify features that would be part of the plasticity phenotype. Eight of the features were significantly correlated with at least one of the first 3 dimensions. A measure associated with the E:I balance, was not significantly correlated with the dimensions and so it was not included in the tSNE or cluster analysis. The E:I measure, however, was used for analyzing the composition of the clusters and as a component of the plasticity phenotype because of the importance of the E:I balance for experience-dependent plasticity.

tSNE dimension reduction and cluster analysis

The average expression for the 8 features (Table 3) was compiled into an mxn matrix, with m columns (m=8) representing the significant features and n rows representing each sample from the 3 V1 regions (central, peripheral, monocular) for 5wk Normal, 5wk MD, RO, BD and

BV animals (n=109). t-distributed stochastic neighbor embedding (t-SNE) was used to reduce this matrix to 2-dimensions (2D). tSNE was implemented in R[40] and the tSNE output was sorted using k-means to assign each sample to a cluster. To determine the optimal number of clusters (k) we calculated the within-groups sum of squares for increasing values of k, fit a single-exponential tau decay function to those data, found the "elbow point" at 4τ which was 6, and used that as the optimal number of clusters. The clusters were visualized by color-coding the dots in the tSNE plot and the composition of the clusters was analyzed.

Table 3: Formulas and Pearson's R correlation between functional indices and principal components. The formulas for each identified feature (Fig 3a-c), kinetics calculation (Fig 3d-f) and PCA Identified feature (Fig 6j), along with corresponding correlation (R^2) values on each of the first 3 principal components. The GluN1:GluA2 and $GABA_AR$ Sum:GlutR Sum were not significantly correlated on any of these 3 components.

Feature	Formula	R^2 Dim 1	R^2 Dim 2	R^2 Dim 3
GluN1:GluA2	(GluA2-GluN1)÷(GluA2 + GluN1)	0.002	0.075	-0.002
GluN2B: GluN2A	(GluN2A - GluN2B)÷ (GluN2A + GluN2B)	0.044	-0.421	0.338
$GABA_A\alpha3$:$GABA_A\alpha1$	($GABA_A\alpha1$ - $GABA_A\alpha3$) ÷ ($GABA_A\alpha1$ + $GABA_A\alpha3$)	-0.176	0.504	0.194
Kinetics				
NDMAR Kinetics	([2A:2B]×50ms)+([2A]×36ms)+([2B]×333ms)) ÷([2A:2B]+[2A]+[2B])	na	na	na
$GABA_AR$ Kinetics	(([α1:α3]×49ms)+([α1]×42.2ms)+([α3]×129ms)) ÷([α1:α3]+[α1]+[α3])	na	na	na
PCA identified Features				
All Protein Sum	(GluA2+ GluN1+ GluN2A + GluN2B + $GABA_A\alpha1$ + $GABA_A\alpha3$ + Synapsin)÷7	0.983	0.134	0.039
GlutR sum	(GluA2+ GluN1+ GluN2A + GluN2B)÷4	0.746	-0.160	0.573
$GABA_AR$ Sum	($GABA_A\alpha1$ + $GABA_A\alpha3$)÷ 2	0.478	0.819	-0.047
$GABA_AR$ Sum:GlutR Sum (EI Index)	(GlutR Sum-$GABA_AR$ Sum)÷(GlutR Sum+$GABA_AR$ Sum)	0.036	-0.064	0.012
$GABA_A\alpha1$: GluN2A index	(GluN2A-$GABA_A\alpha1$)÷(GluN2A+$GABA_A\alpha1$)	0.437	-0.743	-0.070
Glun2B:GluA2	(GluN2B - GluA2)÷(GluN2B + GluA2)	0.058	0.209	-0.798
GluN2A:GluA2	(GluN2A - GluA2) ÷ (GluN2A + GluA2)	0.113	-0.172	-0.643

To facilitate analysis of the tSNE clusters we grouped the BV cases into short-term BV (1hr & 6hr) (ST-BV) or long-term BV (1d, 2d, and 4d) (LT-BV), color-coded the samples by rearing

condition and used different symbols to indicate the V1 region. For each cluster we annotated the composition based on the rearing condition of the samples to create 'subclusters' (e.g. LT-BV 1) that were used for the next analyses.

We evaluated the similarity/dissimilarity among the subclusters by calculating the pairwise correlations (Pearson's R) between subclusters using the features identified by the PCA as input to the R package *rcorr*. The correlations were visualized in a matrix with the cells color-coded to indicate the strength of the correlation[33]. The order of the subcluster in the matrix was optimized using hierarchical clustering and a dendrogram was created based on the pattern of correlations (using R dendextend and seriation packages) so that subclusters with strong correlations were nearby in the dendrogram.

Visualization and comparison of plasticity phenotype

The features identified in the PCA analysis were used to indicate the plasticity phenotype for each of the subclusters. In addition to the 8 significant features, the E:I measure was included in the visualization of the plasticity phenotype. The features were color-coded using grey scale for the 3 protein sum features and a color gradient (red = -1, yellow = 0, green = +1) for the 6 protein indices. The plasticity phenotypes were displayed as a stack of color-coded bars with one bar for each feature. For the subclusters, the plasticity phenotypes were ordered by the dendrogram to facilitate comparison among subclusters that were similar versus dissimilar. We also calculated the plasticity phenotypes for the full complement of normally reared and MD animals and displayed those in a developmental sequence to facilitate age-related comparisons with the recovery subclusters. Finally, we did a bootstrap analysis to determine which features of the plasticity phenotypes were different from 5wk normals and used Bonferroni correction to

adjust the significance for the multiple comparisons. This analysis was displayed 2 ways: first, each of the 9 feature bands for the dendrogram ordered subclusters was color-coded white if it was not different, red if it was greater, and blue if it was less than 5wk normals; second, boxplots were made to show the value for each of the 9 features and to identify the subclusters that were different from 5wk normals.

Statistical analyses

We used bootstrap resampling to estimate the confidence intervals (CI) for each of the recovery groups and Monte Carlo simulation to determine if the 5wk Normal or 5wk MD groups fell outside those CIs. These are modern statistical methods often used with small sample sizes when standard parametric or non-parametric statistical tests are not appropriate. The statistical software package R was used to simulate normal distributions with 1,000,000 points using the mean and standard deviation from the recovery groups (RO, BD, BV). Next, a Monte Carlo simulation randomly sampled with replacement from the simulated distribution n times, where n was the number of observations made from the normal or MD group (e.g., n = 4-19). The resampling procedure was repeated 100,000 times to determine the 95%, 99% and 99.9% CIs. The recovery group was considered significantly different (e.g., $p<0.05$, $p<0.01$ or $p<0.001$) from the normal and MD group if the mean of those groups fell outside the CI for the recovery group.

Bootstrapping was also used to compare if the recovery subclusters identified by tSNE and k-means clustering were different from normal. When a subcluster was significantly greater than normal ($p<0.05$) the boxplot was colored red, when it was less than normal ($p<0.05$) the boxplot

was colored blue, and if not it was not different from normal ($p>0.05$), the boxplot was colored grey.

The p-values for the Pearson's correlations were calculated using the rcorr package[32], and the significance levels were adjusted using the Bonferroni correction for multiple comparisons.

We tested if recovery during BV followed either an exponential decay or sigmoidal pattern by fitting curves to the data using Kaleidagraph (Synergy Software, Reading PA). Significant curve fits were plotted on the graphs to describe the trajectory of recovery.

Results

Analyzing recovery of synaptic proteins: Synapsin

We began analyzing the effects of the 3 recovery treatment conditions by comparing expression of a pre-synaptic marker, synapsin, in the central, peripheral, and monocular regions of cat V1. As we reported previously[23], 5wks MD did not affect expression of synapsin relative to 5wk normals (central: 109%±12%, p=0.2361; peripheral: 106%±9%, p=0.2113; monocular: 100%±8%, p=0.4861, Figure 3a). In contrast, synapsin expression doubled after RO (central: 216%±25%, p<0.0001; peripheral: 197%±13%, p<0.0001; monocular: 241%±19%, p<0.0001), decreased after BD (central: 88%±10%, p=0.0123 vs MD; peripheral:96%±5%, p=0.053 vs MD; monocular: 82%±6%, p<0.0001 vs MD), or had a small decrease in the central region after BV (79%±7%, p<0.0001 vs MD) but normal levels in the rest of V1 (peripheral: 92%±9%, p=0.1474; monocular: 96%±9%, p=0.3185). Interestingly, the loss of synapsin in the central region occurred within 1d of BV (89%±11%, p<0.0001).

Analyzing recovery of synaptic proteins: Glutamatergic receptor subunits

Next, we quantified changes in GluA2 and GluN1 expression in V1. RO promoted a small increase in GluA2 expression compared to normals (central: 112%±8%, p<0.0001; peripheral: 118%±2%, p<0.0001; monocular: 172%±16%, p<0.0001). In contrast, after BD treatment GluA2 was reduced in the binocular regions of V1 (central: 40%±10%, p<0.0001; peripheral: 58%±11%, p<0.0001) but not in the monocular region (88%±17%, p=0.1042 vs MD). BV treatment had variable effects on GluA2. In the central region GluA2 was similar to normal (96%±5%, p=0.2257), but below normal in the peripheral region (75%±5%, p<0.0001) and

fluctuated in the monocular region from below (1hr) (56%±10%, p<0.0001) to above (6hrs) (131%±18%, p=0.0418) then back to below normal levels (2d BV: 71%±12%, p=0.0106; 4d BV: 56%±14%, p=0.0006). This pattern of fluctuations was in the opposite direction to what we found previously when MD was started at 5 weeks of age[27].

After RO, GluN1 expression was below normal in all regions of V1 (central: 73%±10%, p=0.0041; peripheral:67%±3%, p<0.0001; monocular: 65%±14%, p=0.0019, Figure 3c) while after BD it recovered to normal levels (central: 85%±14%, p=0.1908; peripheral: 87%±13%, p=0.1753; monocular: 97%±17%, p=0.4286). BV treatment drove region-specific changes of GluN1 expression with a steady increase centrally (y = 297.43-239.58*exp(-x/11.61), df=25, R^2=0.618, p<0.0001) reaching above normal levels after 4d of BV (128%±11%, p=0.00438), fluctuations in the periphery, and a decline in the monocular region to below normal levels (71%±14%, p=0.0214).

We analyzed expression of the NMDAR subunits, GluN2A and GluN2B (Figure 3d,e), because they regulate ocular dominance and bidirectional synaptic plasticity in V1[17], [21] as well as receptor kinetics[36]. As we reported previously[23], MD reduced GluN2A expression across all of V1 (central: 63%±4%, p<0.0001; peripheral: 58%±6%, p<0.0001; monocular: 76%±11% p<0.0001) while RO promoted recovery of GluN2A to normal levels centrally (89%±10%, p=0.1367) but not in peripheral (65%±3%, p<0.0001) or monocular regions (80%±1%, p<0.0001). In contrast, GluN2A did not recover after BD treatment and declined to less than MDs in the peripheral (24%±2%, p<0.0001) and monocular regions (38%±8%, p<0.0001). BV promoted recovery to normal levels in the central region (4d BV: 129%±23%, p=0.1022), but no recovery in the peripheral region (4dBV: 69%±10%, p=0.0957), and a loss in the monocular region (4dBV: 55%±4%, p<0.0001).

GluN2B expression was less than normal and MD levels after both RO (central: 39%±1%, p<0.0001; peripheral: 41%±3%, p<0.0001; monocular: 43%±2%, p<0.0001) and BD (central: 53%±20%, p=0.0085; peripheral: 52%±8%, p<0.0001; monocular: 72%±18%, p=0.0354). In contrast, BV had little effect on GluN2B expression centrally (4dBV: 103%±16%, p=0.4151), but reduced expression in peripheral (4dBV:77%±9%, p=0.0024) and monocular regions where it changed from above (1hrBV: 124%±14%, p<0.0374) to below normal levels (4dBV: 53%±15%, p<0.0007).

Analyzing recovery of synaptic proteins: GABAergic receptor subunits

Previous studies have shown that $GABA_A$Rs are necessary for starting the CP[41], that $GABA_A\alpha1$ regulates patterns of activity needed for ocular dominance plasticity[20] and that $GABA_A\alpha3$ and $GABA_A\alpha1$ regulate the kinetics of $GABA_A$Rs[37], [42]. For these reasons, we examined how the treatments affected the expression of $GABA_A\alpha1$ and $GAB_A\alpha3$. We found that changes in $GABA_A\alpha1$ expression were greatest after BD with large increases in V1 (central: 180%±50%, p=0.0977 ; peripheral: 297%±31%, p<0.0001, monocular 372%±45%, p<0.0001). In contrast, RO (central: 83%±8%, p=0.0239; peripheral:85%±4%, p=0.0008; monocular: 85%±14%, p=0.0026) and BV (4d BV central: 40%±9%, p<0.0001; peripheral:48%±8%, p<0.0001; monocular: 51%±4%, p<0.0001) reduced $GABA_A\alpha1$ in V1. There was, however, a transient increase in $GABA_A\alpha1$ after 6hrs of BV outside the central region (peripheral:181%±14%, p<0.0001; monocular:242%±19%, P<0.0001). RO had little impact on $GABA_A\alpha3$ expression (central, 76%±15%, p=0.0614) but BD reduced it in the binocular regions (central: 38%±6%, p<0.0001; peripheral: 59%±6%, p<0.0001). BV treatment also left $GABA_A\alpha3$ below normal (central: 48%±15%, p=0.0003, peripheral: 50%±3%, p<0.0001;

monocular: 64%±7%, p<0.0001). Thus, none of the recovery conditions returned expression of all 7 proteins to normal levels in all regions of V1. Instead, there was a complex pattern of changes that did not clearly distinguish which treatment condition best restored a normal pattern.

Analyzing heterogeneity in protein expression and comparing among rearing conditions

We were surprised by the complexity in the pattern of protein changes and wondered if there was an abnormally high degree of heterogeneity in the protein expression. To assess heterogeneity, we calculated an index of dispersion (variance-to-mean ratio, VMR) for each protein and condition and used it to determine if the distributions were under-dispersed (VMR < 1), randomly-dispersed (VMR=1) or over-dispersed (VMR>1). For 5wk normal and RO conditions all proteins were under-dispersed with VMRs <0.3 (Figure 3-1). For the other conditions, the proteins were also under-dispersed except after MD. GluN2B was randomly-dispersed in the monocular region (Figure S3-1), and $GABA_A\alpha1$ was over-dispersed centrally after BD and in the monocular region after 4d BV. This analysis did not find increased heterogeneity that explains the complexity, so we continued to analyze patterns of protein expression starting with pairs of proteins known to have functional interactions.

Analyzing the balance between functionally related pairs of receptor subunits

We calculated a set of indices to assess the effects of recovery treatments on the balance between functionally related pairs of receptor subunits: GluA2:GluN1, GluN2A:GluN2B, and $GABA_A\alpha1$:$GABA_A\alpha3$. In normally developing cat V1 the AMPAR:NMDAR balance still favors GluN1 expression at 5wk[23]. In contrast, MD advanced development of the balance to favor GluA2 in central (0.06±0.09, p=0.044) but not other regions (peripheral: -0.20±0.07, p=0.078; monocular: -0.18±0.05, p=0.16, Figure 4a). RO also advanced the balance to favour GluA2

across all of V1 (central: 0.12±0.06, p<0.0001; peripheral: 0.14±0.04, p<0.0001; monocular:0.29±0.06, p<0.0001) while BD had the opposite effect shifting to more GluN1 than normals (central: -0.49±0.08, p=0.0002; peripheral: -0.33±0.04, p<0.0001). Finally, after 4d of BV the AMPAR:NMDAR favored GluN1 across all of V1 (central: -0.26±0.04, p=0.0004; peripheral: -0.25±0.02, p<0.0001; monocular: -0.25±0.05, p=0.0078).

The composition of the NMDAR affects experience-dependent plasticity and more GluN2B facilitates, while more GluN2A reduces, plasticity. MD changed the 2A:2B balance to more GluN2B and RO and BD changed it again to more GluN2A centrally (RO, 0.28±0.06, p<0.0001; BD, 0.14±0.13, p=0.0001) (Figure 4b) while in the rest of V1 RO also had more GluN2A (peripheral: 0.28±0.027, p<0.0001; monocular: 0.31±0.02, p<0.0001), but BD had more GluN2B (peripheral:-0.22±0.08, p=0.0008, monocular:-0.37±0.10). BV also shifted the 2A:2B balance in the direction of normals but after 4d of BV both the central (-0.01±0.05, p=0.0002) and peripheral regions (-0.02±0.04, p=0.0003) were different from normal.

The subunit composition of the $GABA_AR$ also contributes to regulating experience-dependent plasticity in V1 as the developmental addition of $GABA_A\alpha1$ is needed for ocular dominance plasticity[20]. In the central region, both RO and BV shifted the $GABA_A\alpha1$:$GABA_A\alpha3$ balance to normal levels (RO: 0.07±0.15, p=0.3087, 4d BV: -0.01±0.14, p=0.5005, Figure 4c). BV also had a normal balance in the peripheral region (-0.13±0.08, p=0.1163), but BD drove a large shift to favor more $GABA_A\alpha1$ in all regions of V1 (central:0.50±0.13, p=0.0003; peripheral: 0.63±0.03, p<0.0001; monocular: 0.60±0.02, p<0.0001).

Together, the 3 balances highlight region- and treatment-specific changes suggesting that BV may recover closest to 5wk normal balances, however, BV did not simply reinstate normal balances for these pairs of receptor subunits.

Modeling NMDAR and $GABA_AR$ population kinetics

The subunit composition of NMDARs and $GABA_ARs$ help to regulate the threshold for experience-dependent plasticity, in part by controlling the receptor kinetics[36], [37]. We used that information about receptor kinetics with different subunit compositions to make a model that predicts the average population kinetics for the rearing conditions studied here. First, we transformed the 2A:2B and α1:α3 balances into predicted population kinetics (see Methods) and compared among the groups (Figure 4d,e). The pattern of results is necessarily similar to the balances presented above, however, the predicted kinetics suggests a compression of differences between conditions when the balances shift to favor the mature subunits (2A or α1) versus an accentuation of differences to much slower kinetics when the immature subunits (2B or α3) dominated.

To address how treatment induced changes to both NMDAR and $GABA_AR$ composition might change the relationship between glutamatergic and GABAergic transmission timing we made XY scatterplots of those predicted kinetics (Figure 4f, 4-2). In addition, we analyzed the normal development to identify the range of kinetics predicted for the peak of the CP (Figure 4-1). During normal development (black line) there was balanced progression from slow kinetics at 2wks to progressively faster kinetics through the peak of the CP (Figure 4f- yellow zone, 4-6wks) to reach adult levels. The NMDAR:$GABA_AR$ kinetics for MD, RO and BD fell outside the window predicted by the CP, but in different directions. MD had slower NMDAR (central:

135ms±16ms, p=0.0031; peripheral: 121ms±12ms, p<0.0001; monocular: 146ms±27ms, p=0.0007) but faster $GABA_AR$ kinetics (central: 47ms±0ms, p<0.000l; peripheral:48ms±1ms, p=0.0004; monocular: 51ms±4ms, p=0.3795), RO had faster NMDAR (central:46ms±1ms, p<0.0001; peripheral:46ms±0ms, p<0.0001; monocular:46ms±0ms, p<0.0001) but normal CP range $GABA_AR$ (central:54ms±6ms, p=0.3015; peripheral:51ms±2ms, p=0.1586; monocular:48ms±0ms, p<0.0001), and BD had faster $GABA_AR$ (central:46ms±1ms, p<0.0001; peripheral:44ms±0ms, p<0.0001; monocular:45ms±0ms, p<0.0001) but normal CP range NMDAR kinetics in the central region only (central: 61ms±12ms, p=0.0836; peripheral: 130ms±12ms, p<0.0001; monocular: 155ms±27ms, p<0.0001).

The introduction of BV caused a progressive change in the predicted NMDAR:$GABA_AR$ kinetics suggesting an initial speeding up of the NMDAR kinetics over the first 1d to 2d followed by a slowing of the $GABA_AR$ kinetics, especially in the central region.

Taken together, the predicted NMDAR:$GABA_AR$ kinetics suggest differences among the conditions and BV promoting a normal CP balance but none of the treatments reinstate normal kinetics. Furthermore, the univariate analyses have not identified individual proteins or balances that differentiate BV treatment from RO and BD. To address this problem, we implemented a set of unbiased, multivariate analyses to assess network relationships among the proteins, identify plasticity features, and construct plasticity phenotypes.

Analyzing the pairwise similarity between protein expression profiles

First, we wanted to identify pairs of proteins with similar or opposing expression profiles and compare them among the rearing conditions. For each condition, we collapsed the data from the 3 regions of V1, calculated the matrix of pairwise correlations between the 7 proteins, ordered

the protein correlations using a hierarchical dendrogram, and used 2D heatmaps to visualize the correlations (Figure 5). The order of proteins in the dendrogram indicated which ones had similar (e.g. on the same branch of the dendrogram) or different patterns of expression and the color of the cell illustrated the strength of the correlation. For 5wk normal animals (Figure 5a), there were strong positive correlations (red cells) among all proteins except GluN2A, which was weakly correlated and not clustered with the other proteins. A very different pattern of correlations was found after MD (Figure 5b); here glutamatergic proteins were weakly, or even negatively correlated (blue cells) with $GABA_A\alpha1$, $GABA_A\alpha3$, and synapsin. These results suggest that MD drives a decoupling of these excitatory and inhibitory mechanisms. RO also separated glutamatergic and GABAergic proteins into different clusters at the first branch (Figure 5c); however, the correlations were weaker, suggesting that RO reduced the MD-driven decoupling of these mechanisms. After BD the correlation matrix had mostly positive correlations (Figure 5d) except for synapsin which was negatively correlated and not clustered with the other proteins. BV treatment highlighted the dynamic nature of this recovery (Figure 5e-i). Just 1hr of BV was enough to change the correlation matrix from the MD pattern, but even after 4d of BV the correlation matrix still appeared different from the normal 5wk pattern of correlations.

These matrices revealed different patterns of correlations depending on the condition, but this analysis treats each comparison with the same weighting and it is likely that some proteins contribute more than others to the variance in the data. To assess this, we used PCA to identify individual proteins and combinations of proteins that capture the variance in the data and may represent plasticity features that identify difference among the treatment conditions.

Using principal component analysis to reduce dimensionality and identify plasticity features

We used PCA to reduce the dimensionality, transform the data and find features that define the covariance among the proteins. An *m*x*n* matrix was made using protein expression, where the m columns were the 7 proteins and the n rows (109) were the tissue samples from all the animals and regions of V1 used in this study. This matrix was analyzed using singular value decomposition (SVD), and the first 3 dimensions explained most of the variance (82%) in the data (Dim1: 54%, Dim2: 18%, Dim3: 10%) (Figure 6a).

To understand which proteins contributed to each dimension we addressed the quality of the representation for each protein using the $\cos^2$ metric and found that the glutamatergic proteins were well represented by Dim1, $GABA_A\alpha1$ by Dim2, and GluA2 and GluN2B by Dim3 but synapsin and $GABA_A\alpha3$ were weakly represented in the first 3 dimensions (Figure 6 b,c). Next, we compared the vectors for each protein (Figure 6 d,f) and the PCA space occupied by the rearing conditions (Figure 6 e,g). The protein vectors show that GluN1, GluN2A, GluN2B, and GluA2 extended along Dim1, $GABA_A\alpha1$ along Dim2, and GluA2 and GluN2B were in different directions along Dim3. The PCA space occupied by the conditions identified some differences: BD was separated on Dim 2 in the same direction as $GABA_A\alpha1$, but the center of gravity for the other conditions overlapped the space occupied by normal samples.

The overlap among conditions raised the possibility that higher dimensions may separate the conditions. To begin to assess higher dimensional contributions we examined the basis vectors (Figure 6h) and the correlations between individual proteins and PCA dimensions (Figure 6i) to identify combinations of proteins that might reflect higher dimension features. For example, all

proteins had positive amplitudes for the Dim1 basis vector (Figure 6h) and positive correlations with Dim1 (Figure 6i) suggested that protein sums may be higher dimensional features. In addition, weights for GluN2A and $GABA_A\alpha1$ on Dim2 were opposite, suggesting that when one protein increased the other decreased and this could be a novel feature of these data. Continuing with this approach we identified 9 putative plasticity features; protein sums (all protein sum, GlutR sum, $GABA_AR$ sum) or indices (GlutR:$GABA_AR$, GluN2A:GluN2B, $GABA_A\alpha1$:$GABA_A\alpha3$, GluN2A:$GABA_A\alpha1$, GluA2:GluN2B, GluN2A:GluA2). All of the protein sums and 4 of the indices were features not analyzed with the univariate statistics; however, each had a strong biological basis in previous research. For example, the new indices paired the mature GluN2A with the mature $GABA_A\alpha1$ or GluA2 subunit, and GluN2B with GluA2 which is known to regulate the development of AMPARs[43]. Finally, we calculated the 9 features and determined if at least one of the first 3 dimensions was correlated with the features (Figure 6j). Only the GlutR:$GABA_AR$ balance was not correlated with any of the first 3 dimensions, but because these mechanisms are related to the E:I balance[44] we included this measure in the next analysis.

We plotted the plasticity features and saw that the GlutR and $GABA_AR$ sums identified differences among the treatment conditions. For example, in the central region RO (77%±5%, $p<0.0001$) and BD (66%±14%, $p=0.0078$) had less GlutR but it returned to normal with BV (4dBV= 114%±10%, $p=0.0671$) (Figure 7b). In contrast, $GABA_AR$ decreased for both BV (44%± 12, $p<0.0001$) and RO (80%±7%, $p=0.0029$) but after BD it either did not change (central: 129%±33%, $p=0.1868$) or increased substantially (peripheral: 175%±19, $p<0.0001$ & monocular: 240%±40, $p<0.0001$) (Figure 7c). BV caused a shift of the GlutR:$GABA_AR$ to favor GlutR in central (0.51±0.12, $p=0.0002$) and peripheral V1 (0.33±0.04, $p<0.0001$) while BD

shifted in the other direction to more $GABA_AR$ (central: -0.22±0.12, p=0.0072; peripheral: -0.45±0.05, p<0.0001; Figure 7d). That pattern was mirrored by the GluN2A:$GABA_A\alpha1$ index, with BV shifting to more GluN2A (4dBV central:0.51±0.14, p=0.0004; peripheral: 0.28±0.10, p=0.0484; monocular:-0.22±0.18, p=0.0319) and BD to more $GABA_A\alpha1$ than normal (central: -0.41±0.13, p=0.0038; peripheral: -0.77±0.03, p<0.0001; monocular: -0.78±0.03, p<0.0001) (Figure 7e). The GluN2B:GluA2 index identified RO as different with substantially more GluA2 (central: 0.40±0.02, p<0.0001; peripheral: 0.43±0.04, p<0.0001; monocular: 0.55±0.01, p<0.0001; Figure 7f). Together, these features helped to begin to identify glutamatergic versus GABAergic differences among the treatment conditions.

Using t-SNE to transform and visualize clustering in the pattern of plasticity features

We used t-SNE to transform the plasticity features and visualize them in 2D (Figure 8a), then k-means and the "elbow method" (Figure 8-1) to identify the number of clusters. For these analyses, the BV samples were collapsed into short-term (1-6hr ST-BV) and long-term (1-4d LT-BV) groups, and the plasticity features were calculated for all samples from the 3 V1 regions (central, peripheral, monocular).

Six clusters were visualized with t-SNE (Figure 8) and the composition of the clusters was analyzed to determine the V1 regions and rearing conditions in each cluster. Cluster 1 was the largest with 39 samples (26% central, 54% peripheral, 21% monocular) and had the greatest number of samples from the central region (Figure 8b,d). Cluster 3 also had samples from central, peripheral and monocular regions while clusters 4, 5, and 6 were dominated by peripheral samples with few or no central region samples. Thus, there was some clustering by V1 region, but more apparent clustering emerged when the samples were color-coded by rearing

condition (Figure 8c, d). All but one of the normal samples were in cluster 1, all of the RO samples were in cluster 2, most of the BD samples were in cluster 3 with a few in cluster 6, and most of the MD samples were in clusters 1 or 3. The BV samples, however, were found in 5 of the clusters with the greatest number of BV central samples (83%) grouped with normals in cluster 1.

Further analysis of cluster 1 showed that the majority of central region samples from LT-BV and ST-BV clustered with the normals (Figure 8d). Interestingly, some of the MD samples were also in cluster 1; however, those samples were from the peripheral and monocular regions which are known to be less affected by MD than the central region[45]. Together, these results show that the data are clustered and that the clustering was driven by both rearing condition and region of V1.

Correlating plasticity features among subclusters

We annotated the samples in each cluster using the rearing condition and V1 region and used that information to identify 13 subclusters where at least one region per condition had $n \geq 2$ and >20% of the samples in that cluster (Figure 8d, black font). A correlation matrix was calculated to assess the similarity between subclusters (see Table 9-1 for R values and 9-2 for Bonferroni adjusted p values) and the order of the subclusters in the correlation matrix was optimized by hierarchical clustering so subclusters with similar patterns of features were nearby in the dendrogram. Bonferroni adjusted p value was used to determine the significant correlations (0.05/78=0.0006) (Figure 9). This analysis showed that 3 of the 4 LT-BV subclusters (LT-BV 1: R=0.98; LT-BV 5: R=0.98; LT-BV 4: R=0.96) and the MD 1_{PM} subcluster (R=0.98) were strongly correlated with normals. The other MD subcluster with central samples (MD 3_{CP}) was

on a separate branch of the dendrogram and was strongly correlated with the 3 ST-BV subclusters (ST-BV 1: R=0.98; ST-BV 3: R=0.99; ST-BV 5: R=0.98). The ST-BV subclusters were also correlated with normals (ST-BV 1: R=0.96; ST-BV 3: R=0.94; ST-BV 5: R=0.97), LT-BV 1 (ST-BV 1: R=0.98; ST-BV 3: R=0.94; ST-BV 5: R=0.98), and MD1 (ST-BV 1: R=0.98; ST-BV 3: R=0.94; ST-BV 5: R=0.99) but weaker correlations with LT-BV 4 (ST-BV 1: R=0.94; ST-BV 5: R=0.95) and no significant correlations with LT-BV 5. RO was correlated with normal (R=0.96) but only one of the LT-BV subclusters (LT-BV 5: R=0.96) and none of the ST-BV subclusters. The two BD subclusters were correlated (R=0.94) but none of the other correlations were significant. The pattern of strong correlations in this matrix and the resulting dendrogram suggested that the subclusters might form 4 groups that have similar plasticity features (1: normal, LT-BV, $MD_{P\ or\ M}$; 2: RO; 3: ST-BV, MD_C; 4: BD).

Constructing plasticity phenotypes and comparing among the conditions

To compare the pattern of plasticity features among the subclusters we visualized the average for each feature as a color-coded horizontal band, stacked the bands to illustrate the pattern that we called the plasticity phenotype (Figure 10a) and ordered the phenotypes using the same dendrogram as the correlation matrix (Figure 10b). In addition, we visualized the plasticity phenotypes for normal development and MD to compare the treatment subclusters with a broad range of ages that had developed with either normal or abnormal visual experience (Figure 10 c,d).

Inspection of the plasticity phenotypes identified some obvious and other subtler differences among the subclusters (Figure 10b). Indeed, the pattern of red and green bands in the BD phenotypes was different from 5wk normals (Figure 10) and identified the shift to more

$GABA_A\alpha1$ and less GluN2A. For the RO subcluster, the light grey bands and number of green bands identified loss of protein expression and a shift to more GluN2A than 2B and more GluA2 than 5wk normals. The RO pattern, however, appeared similar to an older (e.g. 12wk) normally reared animal suggesting that RO may accelerate maturation of these proteins. Thus, BD and RO treatments promote distinct plasticity phenotypes.

The pattern of red and green bands in the plasticity phenotype for LT-BV and some of the ST-BV subclusters (ST-BV1, ST-BV5) appeared similar to the 5wk normals (Figure 10b) but many of the features were still significantly different from the age-matched normals (Figure 11a, 11-1). Nonetheless, these subclusters had some consistent differences with less $GABA_ARs$ and more GluN2B than 5wk normals. Interestingly, one of the novel features found by PCA, the GluN2A:GluA2 balance, was the only measure where all of the LT-BV subclusters were not different from 5wk normals but both RO and BD were different. Thus, this visualization of the plasticity phenotypes illustrated that the pattern promoted by BV, and LT-BV in particular, was most similar to the normal CP phenotype, when compared to the adult-like appearance of the RO or unique appearance of the BD phenotype.

Discussion

Here we studied a set of glutamatergic and GABAergic receptor subunits that regulate plasticity and classified their expression patterns when MD was followed by a treatment that causes either persistent bilateral amblyopia (RO or BD) or good acuity in both eyes (BV). We found a complex pattern of changes that varied by treatment and region within V1. Analyzing the balances between receptor subunits and modeling kinetics for NMDAR and $GABA_AR$, however, suggested that BV returns CP-like balances, especially in the central region of V1. Furthermore, PCA and cluster analysis identified higher dimensional features and subclusters with different plasticity phenotypes for the treatments that promote good versus poor recovery of acuity. The LT-BV plasticity phenotypes were closest to the normal CP pattern while the RO phenotype appeared more similar to an adult-like pattern dominated by GluA2. In contrast, the BD phenotypes were dominated by $GABA_A\alpha1$ making it distinct from RO and illustrating that multiple plasticity phenotypes can underlie persistent bilateral amblyopia. Finally, the PCA analysis identified an understudied feature, the balance between mature glutamate receptor subunits (GluN2A:GluA2 balance), as a marker that differentiated treatments supporting good acuity (BV), from those that lead to persistent bilateral amblyopia (RO, BD).

Study design and limitations

The main advantages of the study design include (i) the animal model has excellent spatial vision, including a central visual field, so we could compare changes in regions of V1 that represent different parts of the visual field[27], (ii) the treatments were initiated and completed within the CP[46], (iii) there is detailed information about the recovery of physiology for RO and BV[7], [29], [47], [48] and acuity for all 3 treatments[7], [8], [27], [29], [49], (iv) both RO and

BD cause persistent bilateral amblyopia[8], [49], and (v) the treatments engage different forms of experience-dependent plasticity (RO: competitive; BD: cooperative with degraded visual input; BV: cooperative with normal visual input).

The design used here, however, was limited because unlike the mouse model, it is challenging to apply molecular tools to manipulate specific plasticity mechanisms in cat V1. For example, we observed that one feature (GluN2A:GluA2 balance) identified the LT-BV treatment as similar to normals, but we were not able to manipulate that balance to test its necessity for recovery. In addition, a large number of other treatments have been tested to improve recovery after MD, including a brief period of dark-rearing[49], [50], fluoxetine administration[51], perceptual learning[27], [52], or targeting specific molecular mechanisms (e.g., perineuronal nets[53]) and those were not examined. Undoubtedly, the timing, length, and type of treatment influences recovery but the conditions used here were necessarily limited because of the labor-intensive nature of this study. Notwithstanding these limitations, the plasticity phenotypes identified RO and BD as different from each other and from normals, but the LT-BV subclusters were remarkably similar to the 5wk normal pattern.

The approach took advantage of the reliability and multiplexing capabilities of Western blotting to obtain a large dataset of plasticity proteins from multiple V1 regions and rearing conditions. Western blotting, however, does not provide information about the cell types, layers, cortical columns, or subcellular localization of these proteins that would reveal which circuits are involved in recovery or persistent amblyopia. Even without that information, the application of higher dimensional analyses led to the characterization of features and treatment-based clusters with unique plasticity phenotypes. This phenotyping approach is scalable for studying more proteins or genes, cortical areas, and treatment conditions. Taken together, we think that this

approach can be used in other animal models where molecular tools can be combined with visual testing to identify the features and phenotypes necessary for optimal visual recovery.

BV promoted recovery of CP-like plasticity phenotype and identified GluA2:GluN2A as a balance that differentiated BV treatment

We studied BV treatment because it promotes long-lasting recovery of good acuity in both eyes[27] and those findings are similar to promising results of binocular therapies for treating amblyopia in children[54]. Furthermore, there is good physiological recovery with BV[29], [48]. Thus, it was not surprising to find that LT-BV subclusters had the strongest correlations with normals, or that those subclusters had CP-like phenotypes. However, only one of the features, the GluA2:GluN2A balance, returned to normal levels. These findings suggest that it may not be necessary to recapitulate every detail of the normal phenotype to support good visual recovery and that the GluA2:GluN2A balance may be a characteristic feature for tracking functional recovery. Although that balance is not commonly quantified, both proteins are critical components of mechanisms regulating experience-dependent plasticity in BV animals that balance might signify the adaptive engagement of multiple plasticity mechanisms. For example, the delayed increase in visual responses during ocular dominance plasticity is part of a homeostatic plasticity mechanism regulated by trafficking GluA2-containing AMPARs into the synapse[55], [56]. Meanwhile, the initiation of ocular dominance plasticity requires GluN2A expression[22], and when GluN2A is deleted or reduced MD does not depress deprived eye responses but instead causes enhancement of activity driven by the open eye[21]. Our finding that LT-BV returned a CP-like GluA2:GluN2A balance suggests that BV may prime GluN2A-dependent Hebbian plasticity to consolidate deprived-eye connections while GluA2-dependent homeostatic plasticity enhances deprived-eye responsiveness without triggering runaway

excitation[57]-[61]. Thus, the GluA2:GluN2A balance may reflect the idea that during BV treatment the non-deprived eye acts as a *teacher* guiding both cooperative and competitive plasticity mechanisms[29].

RO promoted an adult-like plasticity phenotype in V1 with more GluA2 and GluN2A

Because RO and BD treatments cause persistent bilateral amblyopia[7], [8], [49] we expected these conditions to have abnormal phenotypes. We were surprised, however, to find very different phenotypes for these conditions, showing that more than one plasticity phenotype can account for persistent acuity deficits.

RO samples were in a single cluster dominated by an overabundance of GluA2 and more GluN2A than 2B. Together those changes made the RO phenotype appear more similar to an adult than the CP pattern. The increase in GluA2 was in sharp contrast to the loss after BV treatment, and suggests that RO may scale up AMPAR-dependent homeostatic mechanisms to drive recovery[25] without engaging NMDAR-dependent mechanisms to consolidate those changes[62]. Since AMPAR-mediated homeostasis promotes rapid but transient gains in responsiveness [25], [55], [63]-[66] this might explain the labile acuity recovered with RO[7], [8]. Interestingly, the increase in GluA2 promoted by RO implicates the dense expression of GluA2-containing synapses at feedback connections onto parvalbumin-positive (PV+) neurons[67]. The feedforward connections onto PV+ neurons may also be involved in RO circuit abnormalities because the labile acuity and early shift to GluN2A after RO are similar to changes found in MeCP2 KOs where an abnormally early shift to GluN2A at synapses onto PV+ neurons that halts acuity development[68], [69]. Taken together, RO may leave behind

feedforward (GluN2A subunits) and feedback abnormalities (GluA2) in PV+ neuron circuits in V1.

BD promoted a plasticity phenotype with an over-expression of $GABA_A\alpha1$ and a shift to more GluN2A

Although various models of neural plasticity predict that decreasing firing rates will enhance plasticity that idea has not translated to using BD treatment to improve recovery from MD[49]. BD during the CP has a range of effects on V1 including enhancing the appearance of cytochrome oxidase blobs[70] and weakening stimulus evoked activity of PV+ neurons[71]. Here we found that BD treatment caused an abnormal increase in the expression of $GABA_A\alpha1$ throughout V1 and a shift to more GluN2A in the central region. $GABA_A\alpha1$ receptors are found on pyramidal cell bodies where PV+ neurons synapse and they serve as regulators of ocular dominance plasticity[20] and the window for coincident spike-time dependent plasticity[24]. A recent study has shown that the loss of PV+ activity caused by BD depends on $GABA_A\alpha1$ mechanisms and that blocking this subunit increases BD-evoked activity allowing for LTP of PV+ neurons[72]. Our observation of increased $GABA_A\alpha1$ expression suggests that BD treatment may further reduce visually evoked activity in V1 that is compounded by the shift to more GluN2A reducing the availability of NMDA-dependent mechanism needed to consolidate visual recovery.

Modeling recovery of NMDAR and $GABA_A$R kinetics

Our modeling of population kinetics suggests that different physiological changes accompany the 3 treatments. During normal development the increases in NMDAR and $GABA_A$R kinetics progress in concert. Physiological studies [73] and our modeling show that this fine balance is

decoupled by MD because the delayed shift to GluN2A has slower NMDAR kinetics but the premature increase of $GABA_A\alpha1$ has faster $GABA_AR$ kinetics. Neither RO or BD treatment corrected that decoupling and the modeling suggests that those treatments accelerate the shift to faster adult-like kinetics for NMDARs after RO or $GABA_ARs$ after BD. Modeling the kinetics for BV treatment identified 2 phases of recovery especially in the binocular regions of V1. First, between 0-2 days of BV there was a rapid increase in the predicted NMDAR kinetics and a similar change during normal development takes 2 weeks. Second, between 2-4 days of BV there was a slowing of the predicted $GABA_AR$ kinetics and that was opposite to the normal developmental increase in kinetics. These sequential phases of BV treatment do not recapitulate normal development. Perhaps the BV-driven increase in NMDAR kinetics needs to reach a certain level before triggering the slowing of $GABA_AR$ kinetics to rebalance these mechanisms. This modeling, however, was based on population data about the expression of the receptor subunits and cannot be extrapolated to individual receptors. Nonetheless, the rapid changes with BV treatment suggest that some aspects of normal development may be missed and it will be important to determine what those are.

How might these plasticity phenotypes be used for developing and testing treatments for persistent amblyopia?

The distinct plasticity phenotypes classified for RO and BD treatments show that multiple neural changes can account for persistent amblyopia and highlight the need to know which mechanisms to target when trying to engage neuroplasticity mechanisms to improve acuity. Whether the treatment should focus on AMPARs, NMDARs, $GABA_ARs$ or some combination of those receptors will depend on the underlying plasticity phenotype. Insights into those questions can be addressed in animal models using modern molecular tools and vision testing but

translating those findings into treatments for humans will depend on non-invasive ways to determine an individual's plasticity phenotype. For example, magnetic resonance spectroscopy has been used to measure changes in glutamate or GABA concentrations after different types of visual experience (e.g. MD[74]) and receptor expression can be quantified by radioligands labeled for SPECT and PET [75]. New molecular imaging techniques hold the promise of greater detail with the ability to measure the concentration of receptor subunits[76]-[78]. That information may be comparable to protein analysis in animals models and suitable for constructing plasticity phenotypes for human V1 to facilitate the translation of new treatments. Furthermore, behavioral paradigms linked with specific plasticity mechanisms (e.g. stimulus-selective response plasticity[79] may further aid in characterizing human plasticity phenotypes. Thus, selecting a treatment to prevent or correct persistent amblyopia may benefit from *in vivo* steps to classify an individual's plasticity phenotype.

Conclusions

Of the treatments for MD studied here, only BV promoted recovery of a CP-like plasticity phenotype in V1. However, the phenotype analysis identified that only one feature, the GluA2:GluN2A balance, returned to normal levels after BV and that balance is noteworthy because the proteins are regulators of homeostatic and Hebbian plasticity, respectively. The modeling of NMDAR and $GABA_AR$ kinetics revealed two stages for BV recovery: a rapid increase in NMDAR kinetics, followed by slowing of the predicted $GABA_AR$ kinetics which together brought that balance into the CP range. Finally, we identified features in the plasticity phenotypes that may help to explain persistent amblyopia, the high levels of GluA2 and GluN2A following RO, and the high level of $GABA_A\alpha1$ after BD treatment. This plasticity phenotyping

approach may be useful for designing and testing treatments to improve recovery from or prevent the development of persistent amblyopia.

References

[1] T. N. Wiesel and D. H. Hubel, "Single-Cell Responses in Striate Cortex of Kittens Deprived of Vision in One Eye," *J. Neurophysiol.*, vol. 26, no. 6, pp. 1003–1017, Nov. 1963.

[2] D. H. Hubel and T. N. Wiesel, "The period of susceptibility to the physiological effects of unilateral eye closure in kittens.," *The Journal of Physiology*, vol. 206, no. 2, pp. 419–436, Feb. 1970.

[3] P. B. Dews and T. N. Wiesel, "Consequences of monocular deprivation on visual behaviour in kittens," *The Journal of Physiology*, vol. 206, no. 2, pp. 437–455, Feb. 1970.

[4] E. E. Birch, D. R. Stager Sr, J. Wang, and A. O'Connor, "Longitudinal changes in refractive error of children with infantile esotropia," *Eye*, vol. 24, no. 12, pp. 1814–1821, Dec. 2010.

[5] D. K. Wallace, Pediatric Eye Disease Investigator Group, A. R. Edwards, S. A. Cotter, R. W. Beck, R. W. Arnold, W. F. Astle, C. N. Barnhardt, E. E. Birch, S. P. Donahue, D. F. Everett, J. Felius, J. M. Holmes, R. T. Kraker, M. Melia, M. X. Repka, N. A. Sala, D. I. Silbert, and K. K. Weise, "A randomized trial to evaluate 2 hours of daily patching for strabismic and anisometropic amblyopia in children.," *Ophthalmology*, vol. 113, no. 6, pp. 904–912, Jun. 2006.

[6] D. E. Mitchell, K. M. Murphy, and M. G. Kaye, "Labile nature of the visual recovery promoted by reverse occlusion in monocularly deprived kittens," *Proc Natl Acad Sci USA*, vol. 81, no. 1, pp. 286–288, Jan. 1984.

[7] K. M. Murphy and D. E. Mitchell, "Bilateral amblyopia after a short period of reverse occlusion in kittens.," *Nature*, vol. 323, no. 6088, pp. 536–538, Oct. 1986.

[8] K. M. Murphy and D. E. Mitchell, "Reduced visual acuity in both eyes of monocularly deprived kittens following a short or long period of reverse occlusion.," *Journal of Neuroscience*, vol. 7, no. 5, pp. 1526–1536, May 1987.

[9] L. N. Cooper and M. F. Bear, "The BCM theory of synapse modification at 30: interaction of theory with experiment," *Nat. Rev. Neurosci.*, vol. 13, no. 11, pp. 798–810, Nov. 2012.

[10] T. K. Hensch, "Critical period plasticity in local cortical circuits.," *Nat. Rev. Neurosci.*, vol. 6, no. 11, pp. 877–888, Nov. 2005.

[11] A. Maffei and G. Turrigiano, "The age of plasticity: developmental regulation of synaptic plasticity in neocortical microcircuits.," *Progress in Brain Research*, vol. 169, pp. 211–223, 2008.

[12] G. B. Smith, A. J. Heynen, and M. F. Bear, "Bidirectional synaptic mechanisms of ocular dominance plasticity in visual cortex," *Philosophical Transactions of the Royal Society B: Biological Sciences*, vol. 364, no. 1515, pp. 357–367, Feb. 2009.

[13] K. Yashiro and B. D. Philpot, "Regulation of NMDA receptor subunit expression and its implications for LTD, LTP, and metaplasticity," *Neuropharmacology*, vol. 55, no. 7, pp. 1081–1094, Dec. 2008.

[14] T. K. Hensch and E. M. Quinlan, "Critical periods in amblyopia.," *Vis. Neurosci.*, vol. 35, p. E014, Jan. 2018.

[15] J. A. Heimel, D. van Versendaal, and C. N. Levelt, "The role of GABAergic inhibition in ocular dominance plasticity.," *Neural Plast.*, vol. 2011, no. 2, pp. 391763–11, 2011.

[16] E. M. Quinlan, D. H. Olstein, and M. F. Bear, "Bidirectional, experience-dependent regulation of N-methyl-D-aspartate receptor subunit composition in the rat visual cortex during postnatal development.," *Proc Natl Acad Sci USA*, vol. 96, no. 22, pp. 12876–12880, Oct. 1999.

[17] B. D. Philpot, A. K. Sekhar, H. Z. Shouval, and M. F. Bear, "Visual Experience and Deprivation Bidirectionally Modify the Composition and Function of NMDA Receptors in Visual Cortex," *Neuron*, vol. 29, no. 1, pp. 157–169, Jan. 2001.

[18] B. D. Philpot, J. S. Espinosa, and M. F. Bear, "Evidence for Altered NMDA Receptor Function as a Basis for Metaplasticity in Visual Cortex," *Journal of Neuroscience*, vol. 23, no. 13, pp. 5583–5588, Jul. 2003.

[19] A. J. Heynen, B.-J. Yoon, C.-H. Liu, H. J. Chung, R. L. Huganir, and M. F. Bear, "Molecular mechanism for loss of visual cortical responsiveness following brief monocular deprivation," *Nature Publishing Group*, vol. 6, no. 8, pp. 854–862, Aug. 2003.

[20] M. Fagiolini, J.-M. Fritschy, K. Löw, H. Möhler, U. Rudolph, and T. K. Hensch, "Specific GABAA circuits for visual cortical plasticity.," *Science*, vol. 303, no. 5664, pp. 1681–1683, Mar. 2004.

[21] K. K. A. Cho, L. Khibnik, B. D. Philpot, and M. F. Bear, "The ratio of NR2A/B NMDA receptor subunits determines the qualities of ocular dominance plasticity in visual cortex.," *Proc. Natl. Acad. Sci. U.S.A.*, vol. 106, no. 13, pp. 5377–5382, Mar. 2009.

[22] M. Fagiolini, H. Katagiri, H. Miyamoto, H. Mori, S. G. N. Grant, M. Mishina, and T. K. Hensch, "Separable features of visual cortical plasticity revealed by N-methyl-D-aspartate receptor 2A signaling.," *Proc Natl Acad Sci USA*, vol. 100, no. 5, pp. 2854–2859, Mar. 2003.

[23] B. R. Beston, D. G. Jones, and K. M. Murphy, "Experience-dependent changes in excitatory and inhibitory receptor subunit expression in visual cortex.," *Front Synaptic Neurosci*, vol. 2, p. 138, 2010.

[24] R. C. Froemke and Y. Dan, "Spike-timing-dependent synaptic modification induced by natural spike trains," *Nature*, vol. 416, no. 6879, pp. 433–438, Mar. 2002.

[25] M. A. Gainey, J. R. Hurvitz-Wolff, M. E. Lambo, and G. G. Turrigiano, "Synaptic scaling requires the GluR2 subunit of the AMPA receptor.," *J. Neurosci.*, vol. 29, no. 20, pp. 6479–6489, May 2009.

[26] K. Iny, A. J. Heynen, E. Sklar, and M. F. Bear, "Bidirectional Modifications of Visual Acuity Induced by Monocular Deprivation in Juvenile and Adult Rats," *Journal of Neuroscience*, vol. 26, no. 28, pp. 7368–7374, Jul. 2006.

[27] K. Williams, J. L. Balsor, S. Beshara, B. R. Beston, D. G. Jones, and K. M. Murphy, "Experience-dependent central vision deficits: Neurobiology and visual acuity.," *Vision Research*, vol. 114, pp. 68–78, Sep. 2015.

[28] K. R. Duffy, D. H. Bukhamseen, M. J. Smithen, and D. E. Mitchell, "Binocular eyelid closure promotes anatomical but not behavioral recovery from monocular deprivation," *Vision Research*, vol. 114, pp. 151–160, Sep. 2015.

[29] P. C. Kind, D. E. Mitchell, B. Ahmed, C. Blakemore, T. Bonhoeffer, and F. Sengpiel, "Correlated binocular activity guides recovery from monocular deprivation.," *Nature*, vol. 416, no. 6879, pp. 430–433, Mar. 2002.

[30] K. M. Murphy and D. E. Mitchell, "Vernier acuity of normal and visually deprived cats.," *Vision Research*, vol. 31, no. 2, pp. 253–266, 1991.

[31] E. B. Hollingsworth, E. T. McNeal, J. L. Burton, R. J. Williams, J. W. Daly, and C. R. Creveling, "Biochemical characterization of a filtered synaptoneurosome preparation from guinea pig cerebral cortex: cyclic adenosine 3':5'-monophosphate- generating systems, receptors, and enzymes," *Journal of Neuroscience*, vol. 5, no. 8, pp. 2240–2253, Aug. 1985.

[32] F. E. Harrell Jr and M. C. Dupont, "The Hmisc Package," *R Package, version*, pp. 2–0, 2006.

[33] G. R. Warnes, B. Bolker, L. Bonebakker, R. Gentleman, W. H. A. Liaw, T. Lumley, M. Maechler, A. Magnusson, S. Moeller, and M. Schwartz, "gplots: various R programming tools for plotting data. R package version 2.17. 0," *Computer software*, 2015.

[34] T. Galili, "dendextend: an R package for visualizing, adjusting and comparing trees of hierarchical clustering.," *Bioinformatics*, vol. 31, no. 22, pp. 3718–3720, Nov. 2015.

[35] M. Hahsler, K. Hornik, and C. Buchta, "Getting things in order: an introduction to the R package seriation," *Journal of Statistical Software*, vol. 25, no. 3, pp. 1–34, 2008.

[36] W. Sun, K. B. Hansen, and C. E. Jahr, "Allosteric Interactions between NMDA Receptor Subunits Shape the Developmental Shift in Channel Properties.," *Neuron*, vol. 94, no. 1, pp. 58–64.e3, Apr. 2017.

[37] M. D. Eyre, M. Renzi, M. Farrant, and Z. Nusser, "Setting the time course of inhibitory synaptic currents by mixing multiple GABA(A) receptor α subunit isoforms.," *J. Neurosci.*, vol. 32, no. 17, pp. 5853–5867, Apr. 2012.

[38] J. G. A. Pinto, K. R. Hornby, D. G. Jones, and K. M. Murphy, "Developmental changes in GABAergic mechanisms in human visual cortex across the lifespan.," *Front Cell Neurosci*, vol. 4, p. 16, 2010.

[39] J. G. A. Pinto, D. G. Jones, C. K. Williams, and K. M. Murphy, "Characterizing synaptic protein development in human visual cortex enables alignment of synaptic age with rat visual cortex.," *Front Neural Circuits*, vol. 9, p. 3, 2015.

[40] J. Donaldson and M. J. Donaldson, "Package 'tsne'," *CRAN Repository*, 2010.

[41] T. K. Hensch, M. Fagiolini, N. Mataga, M. P. Stryker, S. Baekkeskov, and S. F. Kash, "Local GABA circuit control of experience-dependent plasticity in developing visual cortex.," *Science*, vol. 282, no. 5393, pp. 1504–1508, Nov. 1998.

[42] K. J. Gingrich, W. A. Roberts, and R. S. Kass, "Dependence of the GABAA receptor gating kinetics on the alpha-subunit isoform: implications for structure-function relations and synaptic transmission.," *The Journal of Physiology*, vol. 489, no. 2, pp. 529–543, Dec. 1995.

[43] B. J. Hall, B. Ripley, and A. Ghosh, "NR2B Signaling Regulates the Development of Synaptic AMPA Receptor Current," *Journal of Neuroscience*, vol. 27, no. 49, pp. 13446–13456, Dec. 2007.

[44] D. Keith and A. El-Husseini, "Excitation Control: Balancing PSD-95 Function at the Synapse.," *Front Mol Neurosci*, vol. 1, p. 4, 2008.

[45] K. M. Murphy, K. R. Duffy, and D. G. Jones, "Experience-dependent changes in NMDAR1 expression in the visual cortex of an animal model for amblyopia," *Vis. Neurosci.*, vol. 21, no. 4, pp. 1–18, Oct. 2004.

[46] C. R. Olson and R. D. Freeman, "Profile of the sensitive period for monocular deprivation in kittens," *Exp Brain Res*, vol. 39, no. 1, Apr. 1980.

[47] J. A. Movshon, "Reversal of the physiological effects of monocular deprivation in the kitten's visual cortex.," *The Journal of Physiology*, vol. 261, no. 1, pp. 125–174, Sep. 1976.

[48] D. S. Schwarzkopf, V. Vorobyov, D. E. Mitchell, and F. Sengpiel, "Brief daily binocular vision prevents monocular deprivation effects in visual cortex," *Eur J Neurosci*, vol. 25, no. 1, pp. 270–280, 2007.

[49] K. R. Duffy and D. E. Mitchell, "Darkness Alters Maturation of Visual Cortex and Promotes Fast Recovery from Monocular Deprivation," *CURBIO*, vol. 23, no. 5, pp. 382–386, Mar. 2013.

[50] E. M. Quinlan, B. D. Philpot, R. L. Huganir, and M. F. Bear, "Rapid, experience-dependent expression of synaptic NMDA receptors in visual cortex in vivo.," *Nat Neurosci*, vol. 2, no. 4, pp. 352–357, Apr. 1999.

[51] J. F. Maya-Vetencourt, A. Sale, A. Viegi, L. Baroncelli, R. de Pasquale, O. F. O'Leary, E. Castrén, and L. Maffei, "The antidepressant fluoxetine restores plasticity in the adult visual cortex.," *Science*, vol. 320, no. 5874, pp. 385–388, Apr. 2008.

[52] K. M. Murphy, G. Roumeliotis, K. Williams, B. R. Beston, and D. G. Jones, "Binocular visual training to promote recovery from monocular deprivation," *Journal of Vision*, vol. 15, no. 1, pp. 2–2, 2015.

[53] D. Carulli, T. Pizzorusso, J. C. F. Kwok, E. Putignano, A. Poli, S. Forostyak, M. R. Andrews, S. S. Deepa, T. T. Glant, and J. W. Fawcett, "Animals lacking link protein have attenuated perineuronal nets and persistent plasticity," *Brain*, vol. 133, no. 8, pp. 2331–2347, Jul. 2010.

[54] K. R. Kelly, R. M. Jost, Y.-Z. Wang, L. Dao, C. L. Beauchamp, J. N. Leffler, and E. E. Birch, "Improved Binocular Outcomes Following Binocular Treatment for Childhood Amblyopia.," *Invest. Ophthalmol. Vis. Sci.*, vol. 59, no. 3, pp. 1221–1228, Mar. 2018.

[55] M. E. Lambo and G. G. Turrigiano, "Synaptic and Intrinsic Homeostatic Mechanisms Cooperate to Increase L2/3 Pyramidal Neuron Excitability during a Late Phase of Critical Period Plasticity," *Journal of Neuroscience*, vol. 33, no. 20, pp. 8810–8819, May 2013.

[56] B.-J. Yoon, G. B. Smith, A. J. Heynen, R. L. Neve, and M. F. Bear, "Essential role for a long-term depression mechanism in ocular dominance plasticity," *Proc Natl Acad Sci USA*, vol. 106, no. 24, pp. 9860–9865, Jun. 2009.

[57] T. Keck, T. Toyoizumi, L. Chen, B. Doiron, D. E. Feldman, K. Fox, W. Gerstner, P. G. Haydon, M. Hübener, H.-K. Lee, J. E. Lisman, T. Rose, F. Sengpiel, D. Stellwagen, M. P. Stryker, G. G. Turrigiano, and M. C. van Rossum, "Integrating Hebbian and homeostatic plasticity: the current state of the field and future research directions," *Philosophical Transactions of the Royal Society B: Biological Sciences*, vol. 372, no. 1715, p. 20160158, Mar. 2017.

[58] M. A. Gainey and D. E. Feldman, "Multiple shared mechanisms for homeostatic plasticity in rodent somatosensory and visual cortex.," *Philos. Trans. R. Soc. Lond., B, Biol. Sci.*, vol. 372, no. 1715, Mar. 2017.

[59] J. Lisman, "Glutamatergic synapses are structurally and biochemically complex because of multiple plasticity processes: long-term potentiation, long-term depression, short-term potentiation and scaling.," *Philos. Trans. R. Soc. Lond., B, Biol. Sci.*, vol. 372, no. 1715, Mar. 2017.

[60] A. X. Yee, Y.-T. Hsu, and L. Chen, "A metaplasticity view of the interaction between homeostatic and Hebbian plasticity.," *Philos. Trans. R. Soc. Lond., B, Biol. Sci.*, vol. 372, no. 1715, Mar. 2017.

[61] F. Zenke and W. Gerstner, "Hebbian plasticity requires compensatory processes on multiple timescales.," *Philos. Trans. R. Soc. Lond., B, Biol. Sci.*, vol. 372, no. 1715, Mar. 2017.

[62] B. D. Philpot, K. K. A. Cho, and M. F. Bear, "Obligatory Role of NR2A for Metaplasticity in Visual Cortex," *Neuron*, vol. 53, no. 4, pp. 495–502, Feb. 2007.

[63] S.-H. Shi, Y. Hayashi, R. S. Petralia, S. H. Zaman, R. J. Wenthold, K. Svoboda, and R. Malinow, "Rapid Spine Delivery and Redistribution of AMPA Receptors After Synaptic NMDA Receptor Activation," *Science*, vol. 284, no. 5421, pp. 1811–1816, Jun. 1999.

[64] G. G. Turrigiano, K. R. Leslie, N. S. Desai, L. C. Rutherford, and S. B. Nelson, "Activity-dependent scaling of quantal amplitude in neocortical neurons," *Nature*, vol. 391, no. 6670, pp. 892–896, Feb. 1998.

[65] A. Maffei and G. G. Turrigiano, "Multiple Modes of Network Homeostasis in Visual Cortical Layer 2/3," *Journal of Neuroscience*, vol. 28, no. 17, pp. 4377–4384, Apr. 2008.

[66] V. Tatavarty, Q. Sun, and G. G. Turrigiano, "How to scale down postsynaptic strength.," *J. Neurosci.*, vol. 33, no. 32, pp. 13179–13189, Aug. 2013.

[67] R. N. Kooijmans, M. W. Self, F. G. Wouterlood, J. A. M. Beliën, and P. R. Roelfsema, "Inhibitory interneuron classes express complementary AMPA-receptor patterns in macaque primary visual cortex.," *J. Neurosci.*, vol. 34, no. 18, pp. 6303–6315, Apr. 2014.

[68] S. Durand, A. Patrizi, K. B. Quast, L. Hachigian, R. Pavlyuk, A. Saxena, P. Carninci, T. K. Hensch, and M. Fagiolini, "NMDA receptor regulation prevents regression of visual cortical function in the absence of Mecp2.," *Neuron*, vol. 76, no. 6, pp. 1078–1090, Dec. 2012.

[69] S. B. Mierau, A. Patrizi, T. K. Hensch, and M. Fagiolini, "Cell-Specific Regulation of N-Methyl-D-Aspartate Receptor Maturation by Mecp2 in Cortical Circuits," *Biological Psychiatry*, vol. 79, no. 9, pp. 746–754, May 2016.

[70] K. M. Murphy, K. R. Duffy, D. G. Jones, and D. E. Mitchell, "Development of cytochrome oxidase blobs in visual cortex of normal and visually deprived cats.," *Cereb. Cortex*, vol. 11, no. 2, pp. 122–135, Feb. 2001.

[71] B. D. Feese, D. E. Pafundo, M. N. Schmehl, and S. J. Kuhlman, "Binocular deprivation induces both age-dependent and age-independent forms of plasticity in parvalbumin inhibitory neuron visual response properties.," *J. Neurophysiol.*, vol. 119, no. 2, pp. 738–751, Feb. 2018.

[72] M. C. Bridi, R. de Pasquale, C. L. Lantz, Y. Gu, A. Borrell, S.-Y. Choi, K. He, T. Tran, S. Z. Hong, and A. Dykman, "Two distinct mechanisms for experience-dependent homeostasis," *Nature Publishing Group*, p. 1, 2018.

[73] A. Maffei, S. B. Nelson, and G. G. Turrigiano, "Selective reconfiguration of layer 4 visual cortical circuitry by visual deprivation.," *Nat Neurosci*, vol. 7, no. 12, pp. 1353–1359, Dec. 2004.

[74] C. Lunghi, U. E. Emir, M. C. Morrone, and H. Bridge, "Short-term monocular deprivation alters GABA in the adult human visual cortex.," *Curr. Biol.*, vol. 25, no. 11, pp. 1496–1501, Jun. 2015.

[75] W.-D. Heiss and K. Herholz, "Brain receptor imaging.," *Journal of Nuclear Medicine*, vol. 47, no. 2, pp. 302–312, Feb. 2006.

[76] J. van der Aart, M. Yaqub, E. J. M. Kooijman, J. Bakker, J. A. M. Langermans, R. C. Schuit, M. B. M. Hofman, J. A. M. Christiaans, A. A. Lammertsma, A. D. Windhorst, and B. N. M. van Berckel, "Evaluation of the Novel PET Tracer [11C]HACH242 for Imaging the GluN2B NMDA Receptor in Non-Human Primates.," *Mol Imaging Biol*, vol. 14, p. 383, Oct. 2018.

[77] A. Haider, I. Iten, H. Ahmed, A. Müller Herder, S. Gruber, S. D. Krämer, C. Keller, R. Schibli, B. Wünsch, L. Mu, and S. M. Ametamey, "Identification and Preclinical Evaluation of a Radiofluorinated Benzazepine Derivative for Imaging the GluN2B Subunit of the Ionotropic NMDA Receptor.," *J. Nucl. Med.*, p. jnumed.118.212134, Jul. 2018.

[78] S. D. Krämer, T. Betzel, L. Mu, A. Haider, A. M. Herde, A. K. Boninsegni, C. Keller, M. Szermerski, R. Schibli, B. Wünsch, and S. M. Ametamey, "Evaluation of 11C-Me-NB1 as a Potential PET Radioligand for Measuring GluN2B-Containing NMDA Receptors, Drug Occupancy, and Receptor Cross Talk.," *J. Nucl. Med.*, vol. 59, no. 4, pp. 698–703, Apr. 2018.

[79] S. F. Cooke and M. F. Bear, "Stimulus-selective response plasticity in the visual cortex: an assay for the assessment of pathophysiology and treatment of cognitive impairment associated with psychiatric disorders.," *Biological Psychiatry*, vol. 71, no. 6, pp. 487–495, Mar. 2012.

Figure Legends

Figure 1. Study design diagram

Timelines for the rearing conditions used in this studied. **a**. Normal visual experience and monocular deprivation (MD), **b**. treatment conditions (RO, BD, BV) after MD to 5wks. Filled bars indicate that an eye was closed. Black arrows indicate the age of animals used in the study. A timeline for the critical period (CP) in cat visual cortex[46] highlights the peak of the CP between 4-6 weeks of age. **c**. Map of the regions in V1 where tissue samples were taken from representing central (C, n=2), peripheral (P, n=8), and monocular (M, n=2) visual fields. **d**. Representative bands from the Western blots for the 7 proteins quantified in the study and the molecular weights (kDa).

Figure 2. Analysis workflow

The analysis workflow for data in the study. **a**. Immunoblots were quantified using densitometry, **b**. Statistical comparisons were made using Monte Carlo simulation and bootstrap resampling. **c**. Pairwise correlations were calculated for the 7 proteins for each rearing condition. **d**. Next, a series of steps were done beginning with dimension reduction (PCA), **e**. Feature selection, **f**. Cluster visualization based on the features (tSNE), **g**. Correlation between features or the clusters and subclusters, **h**. Construction and visualization of the plasticity phenotypes for each subcluster.

Figure 3. Expression of synaptic proteins in the different regions of visual cortex.

Histograms showing the average expression relative to 5 wk normal animals for the 7 proteins (rows) and 3 regions of V1 (columns), normal 5 wk animals (black bars), animals reared with

MD to 5wks (grey bars), and animals treated with either RO (blue bars) or BD (green bars). Scatter plots showing the average protein expression (red dots) after 1hr to 4d of BV treatment. When the trajectory of protein changes during BV treatment was well-defined by a function, curve fits were applied (red line). Error bars represent standard error of the mean (SEM). Black asterisks represent significant differences relative to 5wk normal, and grey asterisks represent significant differences relative to 5wk MD (*p<0.05,**p<0.01, ***p<0.001). The dotted black line on each graph represents 5wk normal expression. For exact p-values, Pearson's R, and equations for the curve-fits see Table 3-2.

Figure 4. Indices for pairs of receptor subunits and modeling of predicted decay kinetics for a population of NMDARs and $GABA_A$Rs. Histograms and scatter plots showing the average expression of the 3 receptor subunit indices (**a:**GluN1:GluA2, **b:**GluN2B:GluN2A, **c:**$GABA_A\alpha1$:$GABA_A\alpha3$) and predicted population kinetics (**d:**NMDAR, **e:**$GABA_A$R) for the regions of V1 (columns). **f.** The predicted population kinetics are plotted for both $GABA_A$Rs (x-values) and NMDARs (y-values) for normally reared animals age range 2wks-adult with the curve representing the trajectory of the relationship between these features (black dots & line, see Figure 4-1 for normal data). Also, the data are plotted for 5wk MD (grey dot), RO (blue dot), and BD (green dot). The relationship between NMDAR and $GABA_A$R kinetics during BV treatment for 1hr (orange) to 4d (red) is plotted, and the line uses the functions fit to the data in d and e. The conventions are the same as in Figure 3. For exact p-values, Pearson's R, and equations for the curve-fits see Table 4-2.

Figure 5. Visualizing pairwise correlations between proteins. Correlation matrices are plotted showing the strength (saturation) and direction (blue:negative; red:positive) of the pairwise Pearson's R correlations between proteins for each condition **a**. 5wk Normal, **b**. 5wk

MD, **c**. RO, **d**. BD, and **e-i**. BV. The order of proteins was determined using hierarchical clustering so proteins with stronger correlations were nearby in the matrix. Significant correlations are denoted by an asterisk (*p<0.05, **p<0.01, ***p<0.001). For table of Pearson's R values and Bonferroni corrected p-values see Table 5-1.

Figure 6. Identifying plasticity features using principal component analysis **a**.The percentage of variance captured by each principal component by singular value decomposition (SVD) applied using all of the protein expression data. The first 3 principal components capture 54%, 18% and 10% of the variance, respectively, totalling >80% and thus representing the significant dimensions. **b.** The quality of the representation, cos^2, for the proteins is plotted for each dimension (small/white: low cos^2; large/blue: high cos^2) **c**. The sum of cos^2 values for the first 3 dimensions for each protein. **d,e.** Biplots of PCA dimensions 1&2 and **f,g.** 1&3. These plots show the vector for each protein (d,f) and the data (small dots) plus the average (large dots) for each condition with the best-fitting ellipse (e,g). **h.** The basis vectors for dimensions 1-3 showing the amplitude of each protein in the vector. **i.** The strength (circle size) and direction (blue-positive, red-negative) of the correlation (R^2) between each protein and the PCA dimensions. **j.** Correlation between the plasticity features (columns) identified using the basis vectors (see Results) and then PCA dimensions 1-3. Filled cells are significant, bonferroni corrected correlations (green = positive, red = negative). For table of Pearson's R values and significant p-values for these associations see Table 6-1.

Figure 7. Expression of plasticity features identified using principal component analysis. Histograms and scatter plots showing the plasticity features (rows)(except GluN2B:GluN2A shown in Fig. 4) that were identified using the PCA basis vectors (Fig. 6j) and

plotted for each region of V1 (columns). The conventions are the same as in Figure 3. For exact p-values, Pearson's R, and equations for the curve-fits see Table 7-1.

Figure 8. Clustering of samples with similar plasticity features identified using t-Distributed Stochastic Neighbor Embedding (t-SNE) and k-means clustering. a. Using tSNE to visualize clustering of samples (109 tissue samples from animals reared to 5wk normal, 5wk MD, RO, BD and BV) calculated from k-means analysis of the 8 plasticity features identified by PCA. The optimal number of clusters (k=6) was identified by measuring the within groups sum of squares at intervals between 2 and 9 clusters (Figure 8-1) **b.** The content of each cluster was visualized for the region (central, peripheral, monocular) **c**. or treatment condition. **d.** The table summarizes the percentage of samples for each region and condition in Cluster 1-6. For example, 100% of the samples from the central region of V1 in Normal animals were in Cluster 1 while 100% of the samples from all regions of RO were in Cluster 2. This information was used to annotate subclusters based on the cluster membership (1-6), rearing condition, and region of V1.

Figure 9. Visualizing pairwise correlations between treatment subclusters. The matrix is showing the strength (0.6=blue; 1=red) of correlation between the subclusters identified in Fig. 7d and annotated here using the rearing condition, cluster (1-6), and region of V1. Hierarchical clustering was used to order the data so that subclusters with strong correlations were nearby in the matrix. The subclusters formed 5 groups using the height of the dendrogram that is denoted by a change in the color of the dendrogram. The dotted black line in the dendrogram highlights the path to the normal subcluster. The black lines in the matrix identify the 5 groupings of the subclusters. For exact Bonferroni corrected p-values see Table 9-1 and for Pearson's R values see Table 9-2.

Figure 10. Visualizing the plasticity features and phenotypes for each subclusters a. We visualized of the plasticity features as a stack of color-coded horizontal bars that together comprise the plasticity phenotype. The 3 grey scale bars represent the protein sums and the 6 red-green color-coded bars represent the protein indices identified by the PCA. **b.** The plasticity phenotypes were calculated for each subcluster and ordered using the same dendrogram as described in Fig. 9. **c**. For comparison the plasticity phenotypes were calculated using previously published data[23] for normal development (2 - 32 wks) **d.** and animals MDed from eye open until either 4, 5, 6, 9 or 32 wks.µµ

Figure 11. Significant plasticity features. a. We used bootstrap analysis to identify plasticity features that were significantly different from 5wk normal animals and color-coded the horizontal bars red if the feature was >normal and blue if it was <normal ($p<0.05$). b-j. The boxplots show the average protein sum (b-d) and an average index value (e-j) for each of the subclusters. Boxes were colored red if significantly greater than 5wk normals, blue if significantly less than 5wk normals and grey if not significantly different from 5wk normals. For exact Bonferroni corrected p-values see Table 11-1.

Extended Data Figure Legends

Figure 3-1. Glutamatergic protein variance to mean ratios. Histograms depict the variance-to-mean ratio in each condition for individual proteins (rows) in each cortical area (columns). VMR >1 represent proteins that are highly-dispersed, VMR=1 are normally dispersed and VMR<1 are under-dispersed.

Figure 4-1. Predicted decay kinetics of NMDAR and $GABA_AR$ across normal cat V1 development Scatterplots of predicted population decay kinetics of each receptor type. Black circles represent the average predicted decay kinetics at each age. Top row of scatterplots show the average kinetics of NMDA receptors across V1 areas. Solid line represents the kinetics of a population of diheteromeric 2A:2B containing NMDARs (50ms). Bottom row shows predicted decay kinetics of GABA receptors across V1 areas. Solid line represents the kinetics of a population of diheteromeric α1:α3 containing $GABA_ARs$ (49ms). All scatterplots were well defined by an exponential decay curve fit (all $p<0.0001$).

Figure 8-1 Within group sum of squares with variable cluster sizes. Scatterplot of the within groups sum of squares was measured across a range of clusters between 2 and 15. An exponential decay fit was applied to the data, and 4τ was taken as the point at which changes in cluster number had little effect on the within groups sum of squares. The optimal number of clusters was identified as 6 (k=6). This value was used to assign the k-means clusters on tSNE reduced data (Figure 8a).

Extended Tables Legends

Table 2-1: The number of tissue samples and runs for Normal animals across V1 region and protein. Rows summarize the number of runs from the Central (C), Peripheral (P), and Monocular (M) regions of V1 within each age of animal studied. The columns list each of the 7 proteins analyzed using Western blotting. Column sums detail the number of runs across ages and cortical areas.

Table 2-2: The number of tissue samples and runs for MD animals across V1 region and protein. Rows summarize the number of runs from the Central (C), Peripheral (P), and Monocular (M) regions of V1 within each age of animal studied. The columns list each of the 7 proteins analyzed using Western blotting. Column sums detail the number of runs across ages and cortical areas.

Table 3-2. Table of p-values comparing protein expression in each treatment condition against 5wk Normal animals and 5wk MD animals. P-values are presented for each cortical area (columns) and protein (rows). Cortical areas are broken up into comparisons against normal (left) and MD (right). Asterisk color coding matches Figure 3. When a curve fit was applied, the equation, degrees of freedom (df), R^2 value and exact p-value are listed.

Table 4-2. Table of p-values comparing the values for each plasticity feature in treatment conditions against 5wk Normal animals or 5wk MD animals. p-values are presented for each cortical area (columns) and plasticity feature (rows). Cortical areas are broken up into comparisons against normal (left) and MD (right). Asterisk color coding matches Figure

4. When a curve fit was applied, the equation, degrees of freedom (df), R^2 value and exact p-value are listed.

Table 5-1. Pearson's R values in each treatment condition comparing the strength of association between each protein. The correlation between each protein within a treatment condition was measured (left), and the observed R values are presented in a matrix. This matrix was reordered in Figure 5 to position high R values nearest one another. The Bonferroni corrected p-values (right) were used to identify the most significant correlations between proteins. P-values <0.05 are colored red to simplify identification of significant correlations.

Table 6-1. Pearson's R correlations between newly identified plasticity features and PCA dimensions. The correlation between the PCA scores across all animals, and the first 3 PCA dimensions are presented. P-values of correlations that were significantly correlated after Bonferroni correction are colored red.

Table 7-1 p-values comparing the each newly identified plasticity feature in treatment conditions against 5wk Normal animals and 5wk MD animals. p-values are presented for each cortical area (columns) and plasticity feature (rows). Cortical areas are broken up into comparisons against normal (left) and MD (right). Asterisk color coding matches Figure 4. When a curve fit was applied, the equation, degrees of freedom (df), R^2 value and exact p-value are listed.

Table 9-1 Pearson's R values comparing the strength of association between each treatment subcluster. The correlation between each sub-cluster was measured and the observed R values are presented in a matrix. This matrix was reordered in Figure 9 to position high R values nearest one another.

Table 9-2 Bonferroni corrected p-values between each treatment subcluster. The Bonferroni corrected p-values were used to identify the most significant correlations between proteins. P-values less than the Bonferroni corrected level (0.0006) are colored red to simplify identification of significant correlations.

Table 11-1. p-values for each identified plasticity feature within subclusters compared against the Normal animals from cluster 1.

p-values are presented for the Pearson's R correlations between each plasticity phenotype and the Normal subcluster. The corresponding significance level is indicated by the text color red if the value was significantly above the normal subcluster, and blue if the value was significantly below, and white if not significantly different.

Figure 1

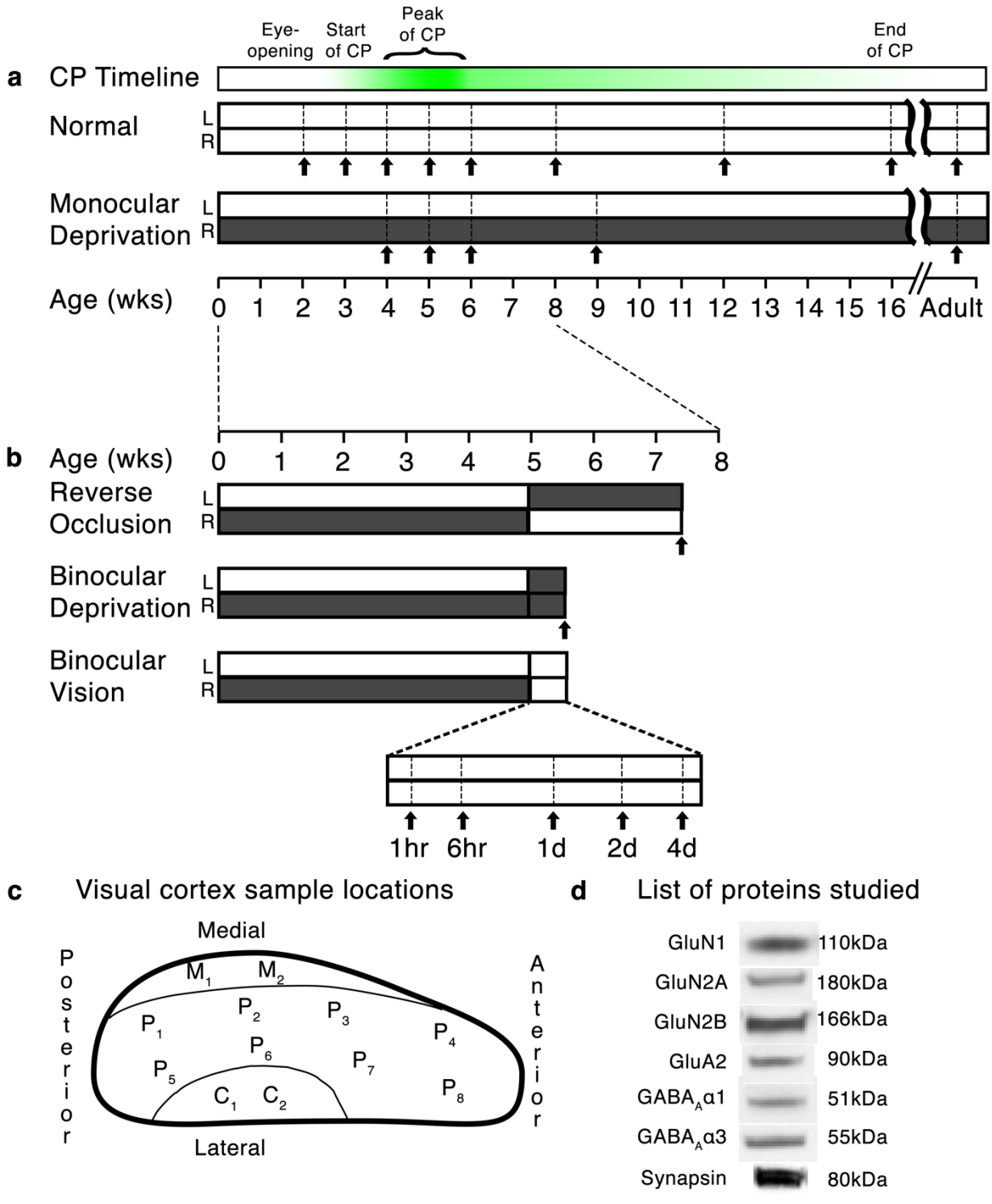

Figure 2

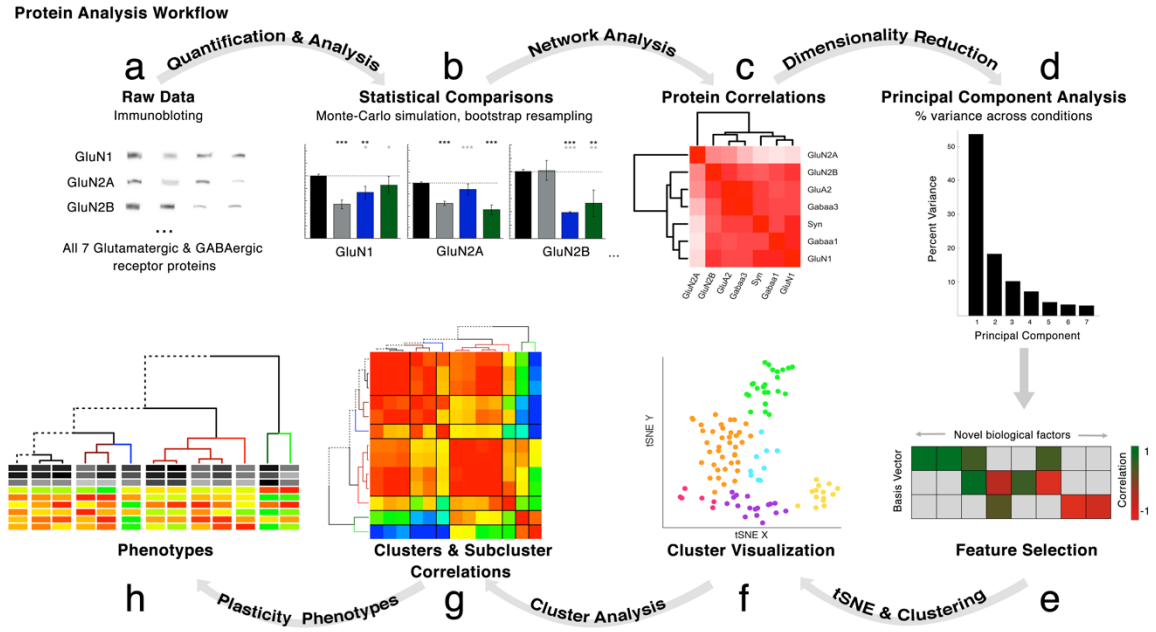

Figure 3

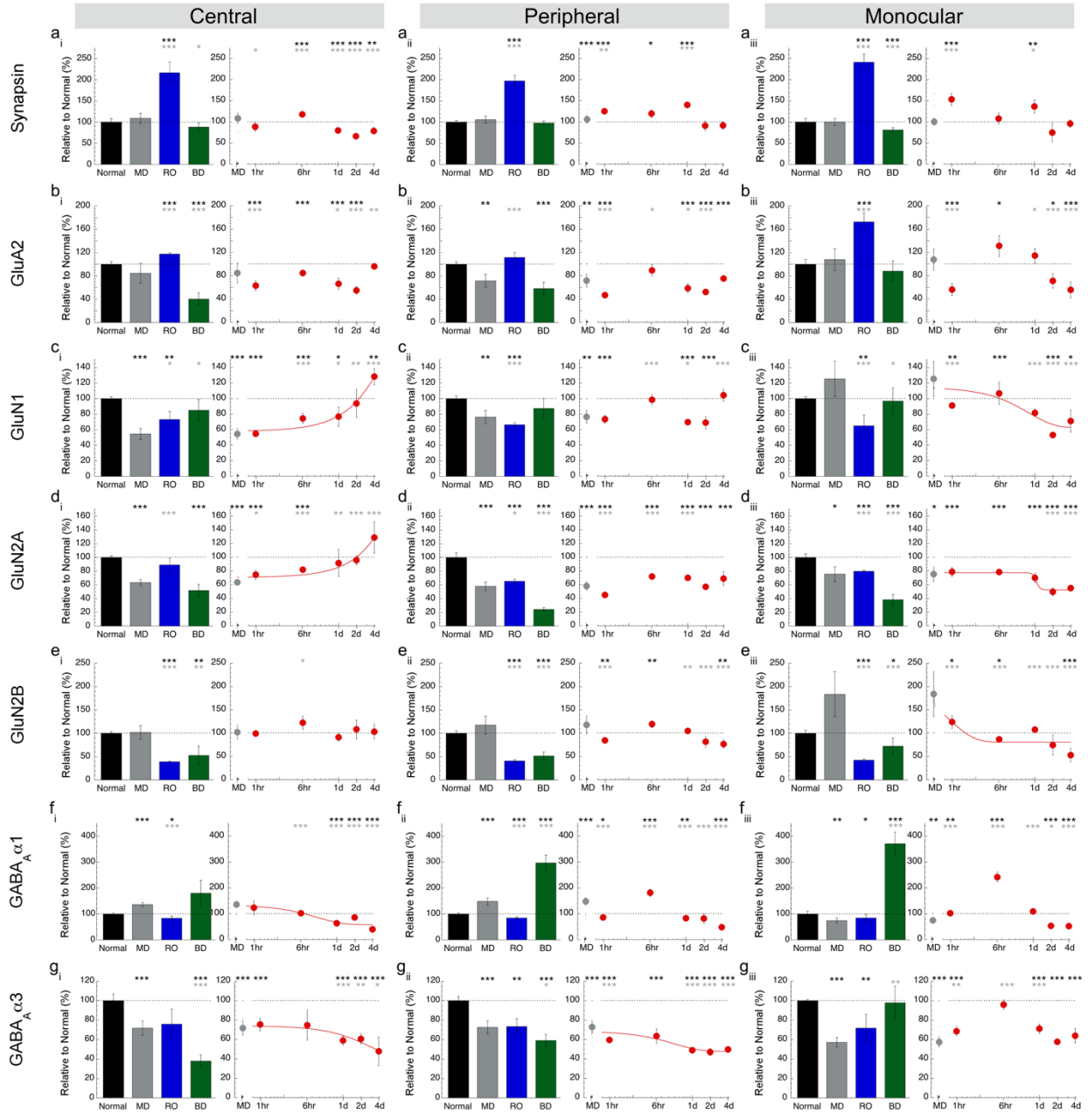

Figure 4

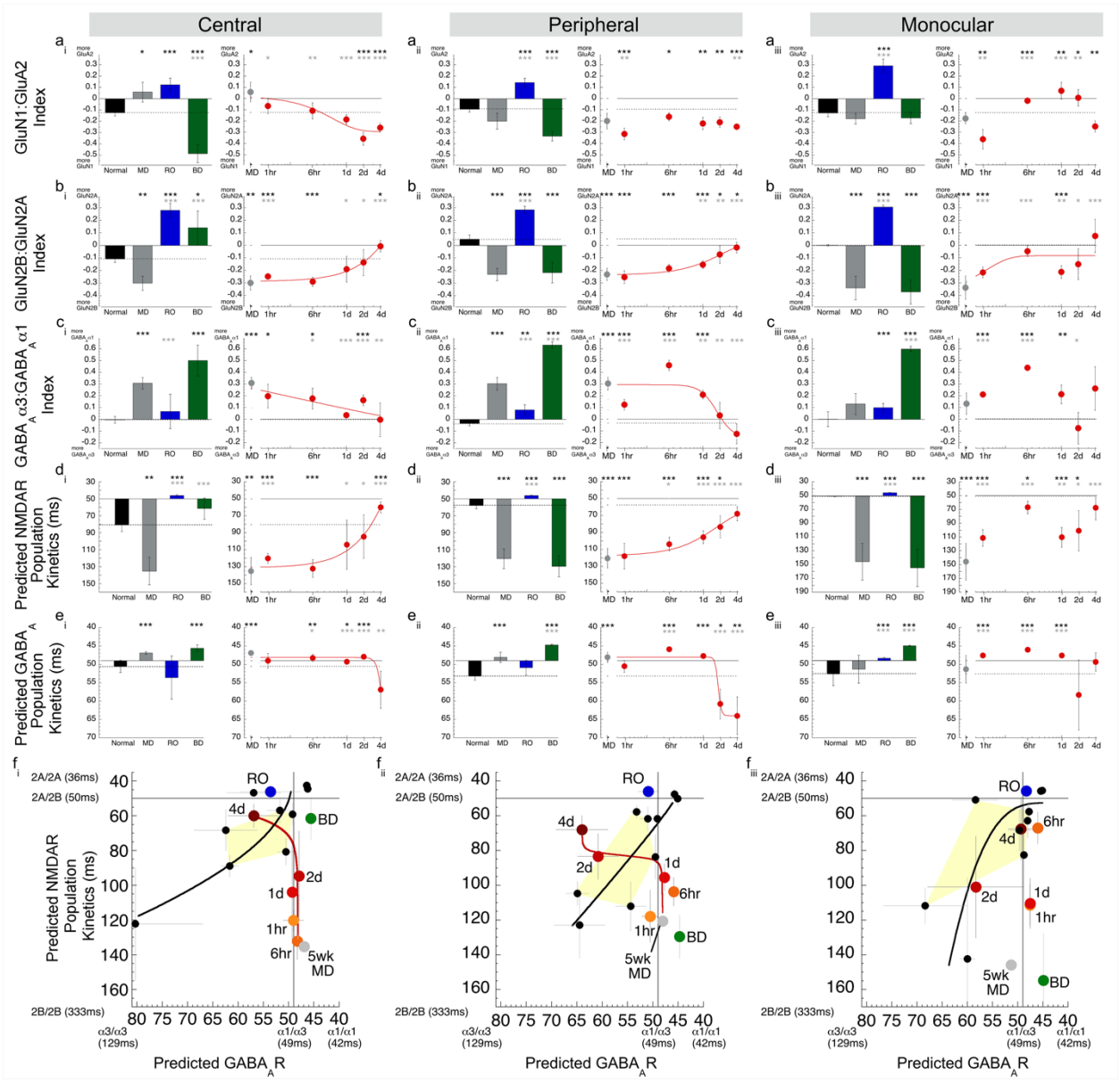

Figure 5

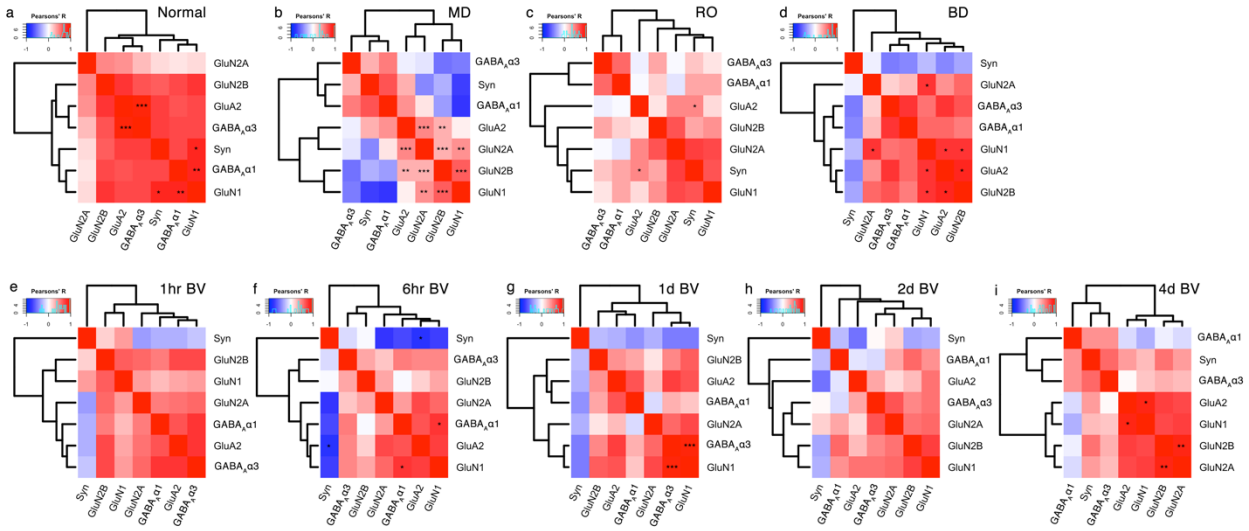

Figure 6

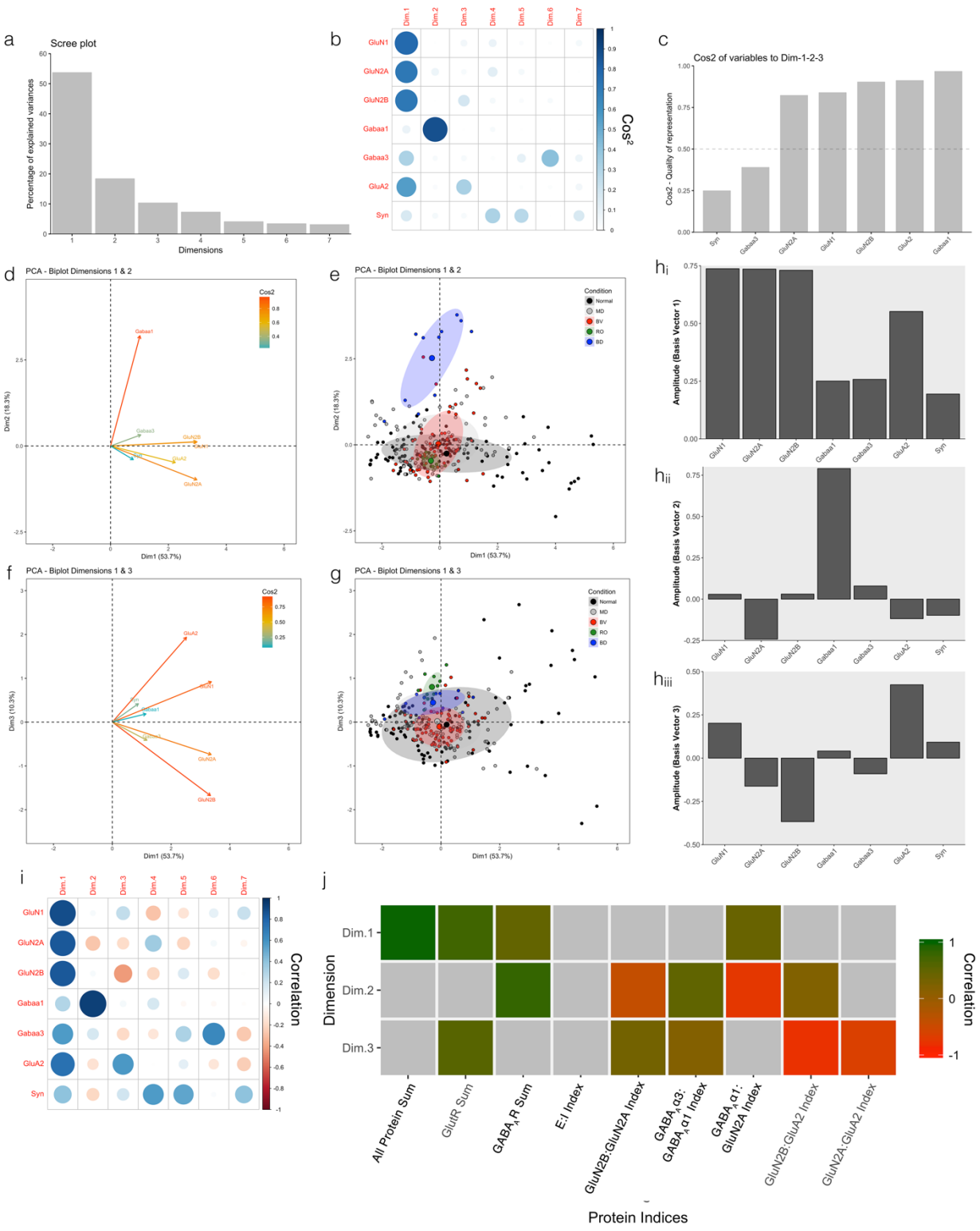

Figure 7

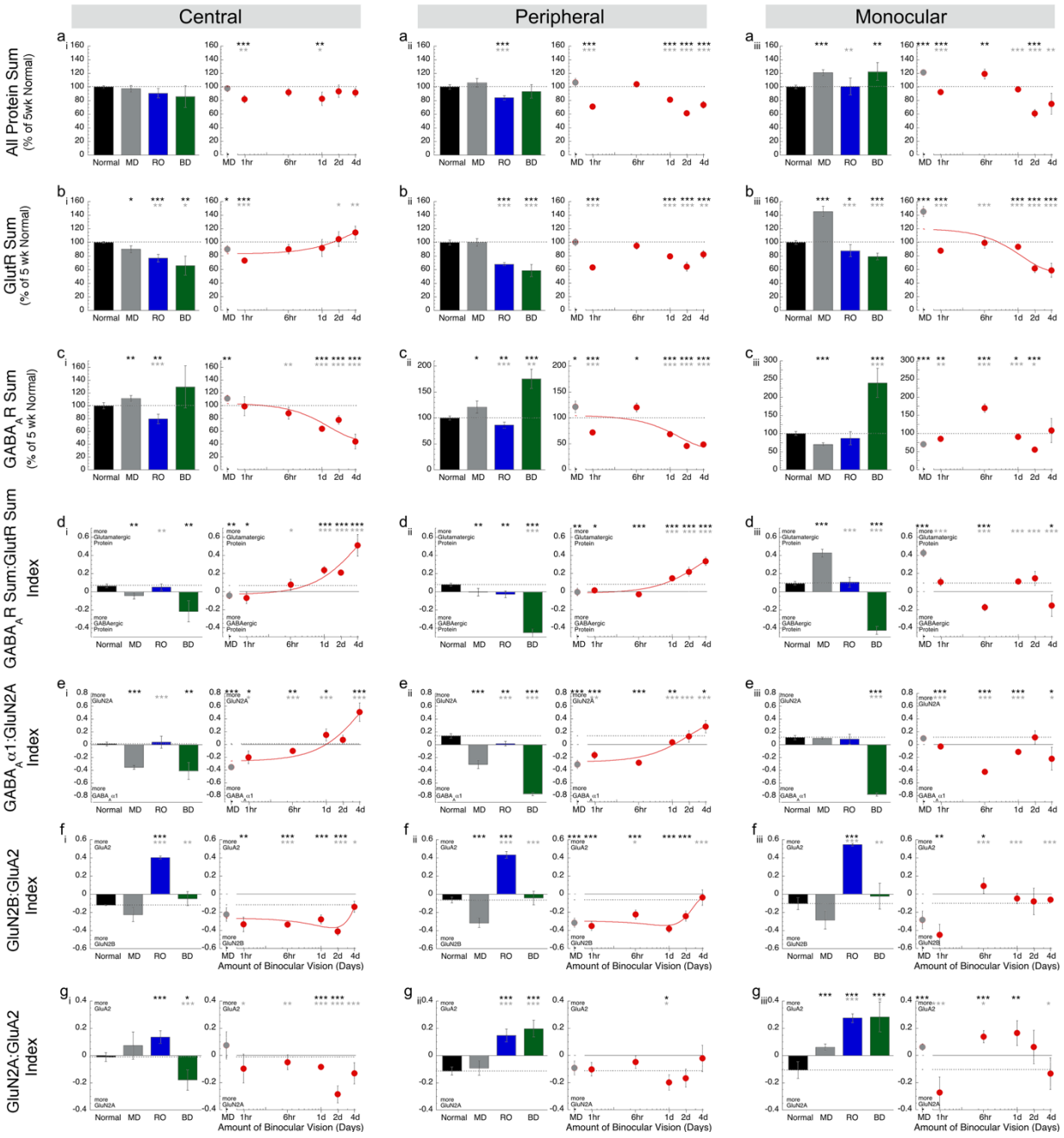

Figure 8

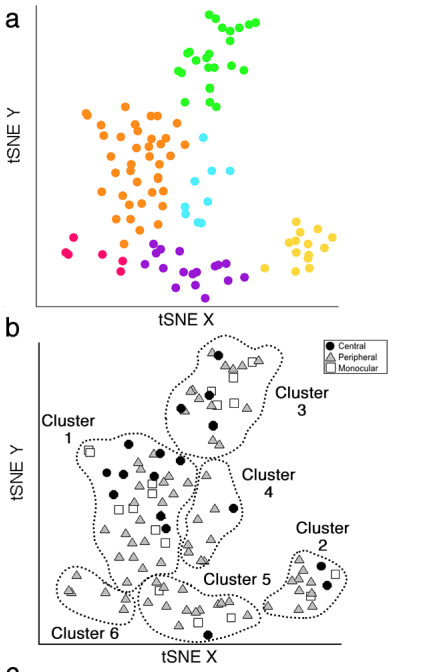

d

		Normal	MD	ST BV (1-6 h)	LT BV (1-4 d)	BD	RO
Cluster 1	C	100		75	83		
	P	88	50	31	27		
	M	100	100	50	33		
Cluster 2	C						100
	P						100
	M						100
Cluster 3	C		100	25		67	
	P		33	31		67	
	M			50	17	100	
Cluster 4	C				17		
	P	13	17	6	23		
	M						
Cluster 5	C					33	
	P			25	41		
	M				50		
Cluster 6	C						
	P			6	9	33	
	M						

Figure 9

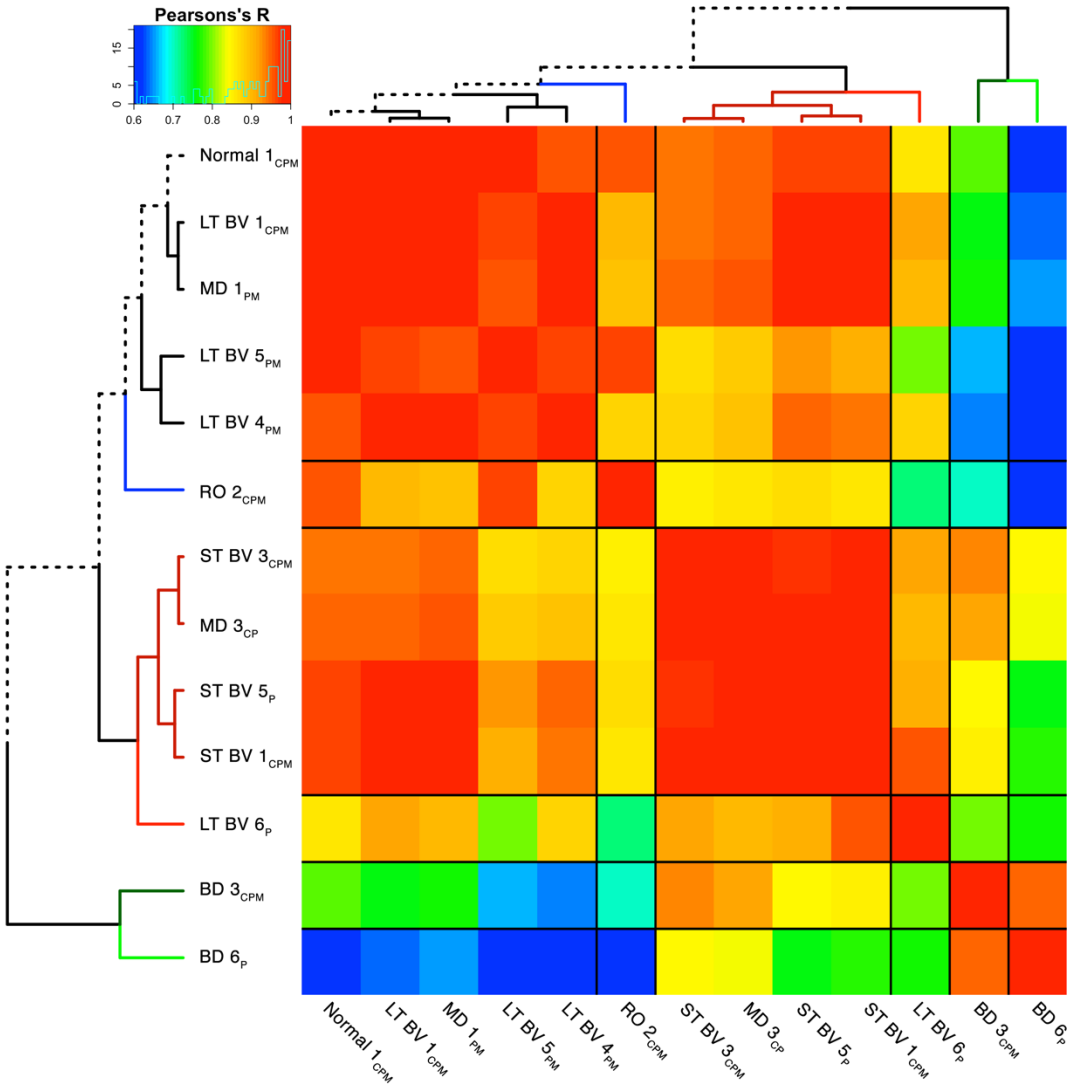

Figure 10

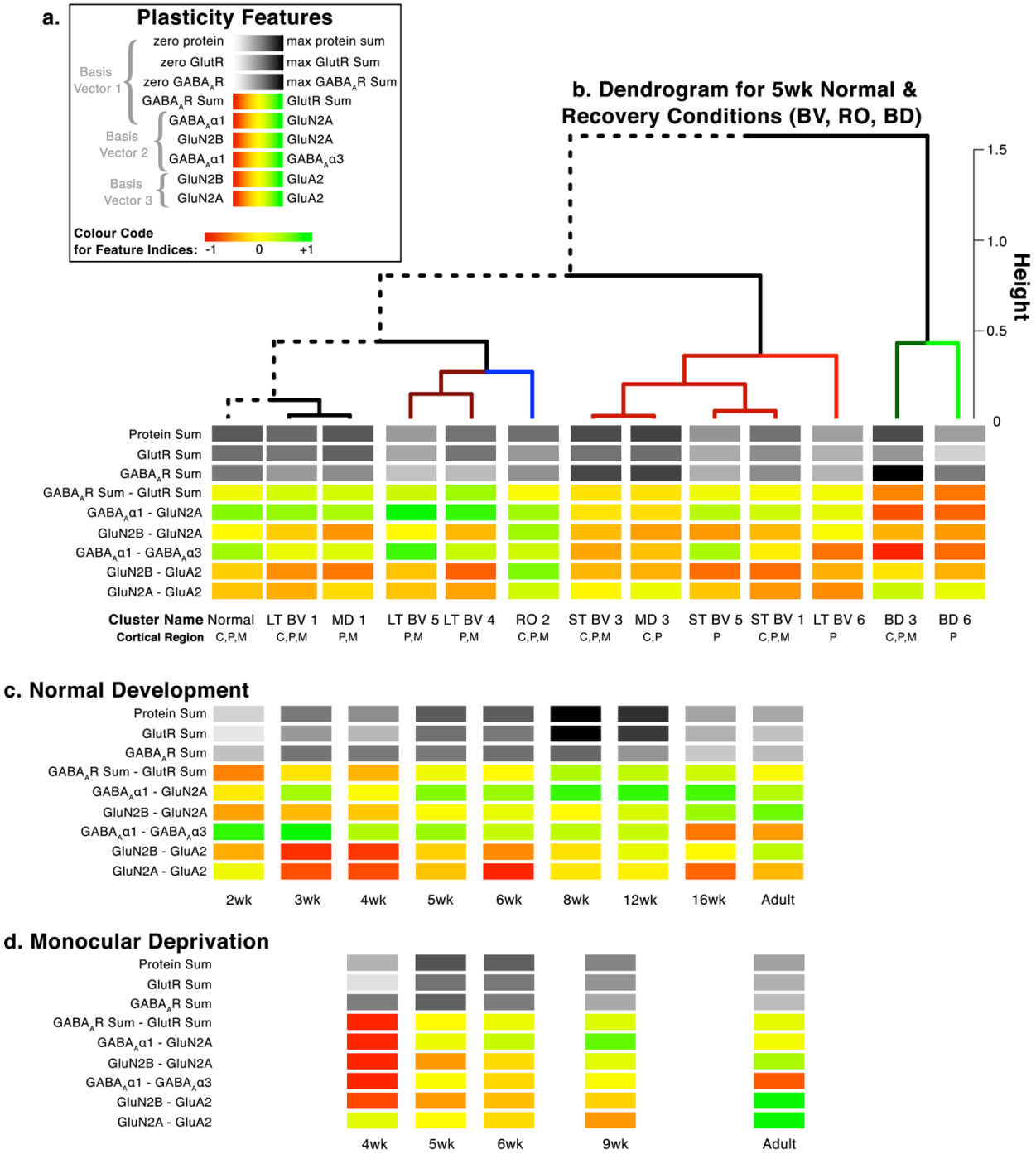

Figure 11